Tectono-stratigraphic evolution of salt-controlled minibasins in a fold and thrust belt, the Oligo-Miocene central Sivas Basin

Charlie Kergaravat, Charlotte Ribes, Jean-Paul Callot, Jean-Claude Ringenbach

Elsevier Editorial System(tm) for Journal of Structural Geology

Manuscript Draft

Manuscript Number:

Title: Tectono-stratigraphic evolution of salt-controlled mini-basins in a fold and thrust belt, the Oligo-Miocene central Sivas basin.

Article Type: Full Length Article

Keywords: Salt tectonics, minibasins, shortening, halokinetic sequences, Sivas Basin.

Corresponding Author: Dr. charlie kergaravat,

Corresponding Author's Institution: University of Pau UPPA

First Author: charlie kergaravat

Order of Authors: charlie kergaravat; Charlotte Ribes; Jean-Paul Callot; Jean-Claude Ringenbach

Abstract: The Central Sivas Basin (Turkey) provides an outcrop example of a minibasin province developed above a salt canopy within a foreland-fold and thrust belt. Several minibasins are examined to assess the influence of regional Oligo-Miocene shortening during the development of a minibasin province. The results are based on extensive field work, including regional and detailed outcrop mapping of at least 15 minibasin margins and analysis of the structural elements at all scales. This reveals a progressive increase in shortening and a decrease in salt tectonics during evolution of the province. The initiation of minibasins is driven mostly by the salt-induced accommodation forming a polygonal network of salt structures with mainly local halokinetic sequences (i.e. hooks and wedges). The intitiation of shortening is marked by an abrupt increase in sedimentation rate within the flexural foreland basin causing burial of the preexisting salt structures. Orogenic compression encourages the rejuvenation of linear salt structures oriented at right angle to the regional shortening direction. The influence of orogenic shortening during the last steps of the minibasin province evolution is clearly shown by: (i) the squeezing of salt structures to form welds which are developed both at right angle and oblique to the regional shortening direction, (ii) the emergence of thrust faults, (iii) the tilting and rotation of minibasins about vertical axis associated with the formation of strike-slip fault zones, and (iv) the extrusion of salt sheets. The pre-shortening geometry of the salt structures pattern, polygonal versus linear salt walls, influence the resultant structural style of the minibasin province subjected to shortening. The thickness of the salt canopy, i.e. "the quantity of salt remobilized", which decreases during minibasin province development, appears to be a major factor controlling the impact of the regional shortening during salt province development.

Dr. Charlie Kergaravat
LFCR
Université de Pau et des Pays de l'Adour
Avenue de l'Université BP 1155
64013 PAU Cedex
FRANCE
charlie.kergaravat@univ-pau.fr
+33 6 23 14 45 12

Pau, 2017 April 19th

To *Journal of Structural Geology* Editors,

Dear Editors,

Please find enclosed a manuscript entitled "**Tectono-stratigraphic evolution of salt-controlled minibasins in a fold and thrust belt, the Oligo-Miocene central Sivas basin**" that I submit to *Journal of Structural Geology* for publication. Authors of this study are myself Charlie Kergaravat (to whom correspondence should be addressed), Charlotte Ribes, Jean-Paul Callot and Jean-Claude Ringenbach.

This manuscript treat of the tectono-sedimentary analysis of the Sivas mini-basins in a context of fold-and-thrust belt. The results are based on extensive field work, including regional and detailed outcrop mapping of at least 15 mini-basins margins and analysis of the structural elements at all scales, integrating previous sedimentological and lithostratigraphic data analyses of outcrops with great details along the tilted mini-basins margins reveal the complex interaction between salt tectonics and sedimentation leading to typical salt-related structures such as: hook and wedge halokinetic sequences, tabular and tapered composite halokinetic sequences, megaflap, allochthonous salt sheets and encapsulated mini-basins.

The minibasins structures are analysed to assess the influence of regional Oligo-Miocene shortening during the development of the minibasin province. This reveals a progressive increase in shortening and a decrease in salt tectonics during evolution of the province. The pre-shortening geometry of the salt structures pattern, polygonal versus linear salt walls, influence the resultant structural style of the mini-basin province subjected to shortening. The thickness of the salt canopy, i.e. "the quantity of salt remobilized", which decreases during mini-basin province development, appears to be a major factor controlling the impact of the regional shortening during salt province development. We develop a new tectono-stratigraphic model for the evolution of the Sivas mini-basin province, and provide a better understanding of the interaction between halokinesis and regional tectonics on the mini-basin development.

Due to the nature of our results and since they provide useful material for further studies of tectono-sedimentary evolution of mini-basins in compressive setting, we think that *Journal of Structural Geology* is the most suitable medium in which these new results can be published.

The study under consideration is an original work, not published elsewhere or under consideration for publication elsewhere. All authors have seen the manuscript and agree to its submission to *Journal of Structural Geology*.

In its present shape, the paper is composed of a main text and 17 figures. Please let me know if anything is wrong in the files I joint to this letter. If necessary, I'll do immediately for the best to improve the submission shape of this manuscript.

Sincerely,

Charlie Kergaravat

Highlights

- Field work data used to examine influence of shortening on minibasin province
- Oligo-Miocene minibasins present an increasing number of shortening evidences
- Minibasins initiation is driven mostly by the salt-induced accommodation
- Minibasins are finally tilted and rotated about vertical axes
- Pre-existing evaporite wall network influences the lateral mobility of the minibasins

Tectono-stratigraphic evolution of salt-controlled minibasins in a fold and thrust belt, the Oligo-Miocene central Sivas basin.

Charlie Kergaravat *,†, Charlotte Ribes *,†,‡ , Jean-Paul Callot* and Jean-Claude Ringenbach†.

* IPRA-LFCR, UMR 5150 CNRS, Université de Pau et des Pays de l'Adour, Pau Cedex, France
† Total SA, CSTJF, Pau, France
‡ Present adress: IPGS-EOST, UMR 7516 CNRS, Université de Strasbourg, Strasbourg, France

Corresponding author: charlie.kergaravat@univ-pau.fr

Keywords: Salt tectonics, minibasins, shortening, halokinetic sequences, Sivas Basin.

ABSTRACT

The Central Sivas Basin (Turkey) provides an outcrop example of a minibasin province developed above a salt canopy within a foreland-fold and thrust belt. Several minibasins are examined to assess the influence of regional Oligo-Miocene shortening during the development of a minibasin province. The results are based on extensive field work, including regional and detailed outcrop mapping of at least 15 minibasin margins and analysis of the structural elements at all scales. This reveals a progressive increase in shortening and a decrease in salt tectonics during evolution of the province. The initiation of minibasins is driven mostly by the salt-induced accommodation forming a polygonal network of salt structures with mainly local halokinetic sequences (i.e. hooks and wedges). The intitiation of shortening is marked by an abrupt increase in sedimentation rate within the flexural foreland basin causing burial of the preexisting salt structures. Orogenic compression encourages the rejuvenation of linear salt structures oriented at right angle to the regional shortening direction. The influence of orogenic shortening during the last steps of the minibasin province evolution is clearly shown by: (i) the squeezing of salt structures to form welds which are developed both at right angle and oblique to the regional shortening direction, (ii) the emergence of thrust faults, (iii) the tilting and rotation of minibasins about vertical axis associated with the formation of strike-slip fault zones, and (iv) the extrusion of salt sheets. The pre-shortening geometry of the salt structures pattern, polygonal versus linear salt walls, influence the resultant structural style of the minibasin province subjected to shortening. The thickness of the salt canopy, i.e. “the quantity of salt remobilized”, which decreases during minibasin province development, appears to be a major factor controlling the impact of the regional shortening during salt province development.

1. INTRODUCTION

In compressive regime, the preferential squeezing of salt structures exerts a powerful control on the resulting deformation and structural style of the fold-and-thrust belt (e.g. Letouzey et al., 1995 ; Vendeville and Nilsen, 1995; Rowan and Vendeville, 2006; Dooley et al., 2009; Jahani et al., 2009; Callot et al., 2012). Existing field studies were focused on preexisting diapirs and salt-withdrawal minibasins developed in rifted, cratonic or passive margin setting which have been uplifted by later shortening, including the Great Kavir (Jackson et al., 1990); the Axel Heiberg Island Artic Canada (Jackson and Harrison, 2006; Harrison and Jackson, 2014) ; the Flinders Ranges (Rowan and Vendeville, 2006; Kernen et al., 2012 ; Hearon et al., 2015), the High Atlas (Saura et al., 2014; Martín-Martín et al., 2017) ; the South Pyrenean foreland (López-Mir et al., 2015; Saura et al., 2015); the French Alps (Graham et al., 2012) and the Zagros fold belt (Sherkati et al., 2006; Jahani et al., 2009; Callot et al., 2012). However, relatively few examples of minibasins province evolving in synchronous shortening, such as at the toe of continental margins, have been described in the literature (e.g. Peel et al., 1995; Brun and Fort, 2004; Dooley et al., 2013; Kergaravat et al., 2016; Duffy et al., 2017).

The Sivas Basin in central Anatolia, Turkey, (Fig. 1a) is a minibasin province showing Wall and Basin (WAB) structures (Harrison and Jackson, 2014) and the presence of two generations of minibasin enveloped by a salt canopy and developed in a foreland fold-and-thrust belt (e.g. Ringenbach et al., 2013; Callot et al., 2014; Ribes, 2015; Kergaravat et al., 2016). It has been proposed that the impact of regional shortening on minibasins was (i) to modify the volume, sorting and composition of the clastic input, (ii) to modify the flexural subsidence and thus the relative influence of localized salt relative accommodation with

respect to regional tectonic accommodation, and (iii) to tilt some of them and weld the contacts.

This last point, i.e. the expression of shortening within the minibasin province has not been described in detail (e.g. Ribes, 2015; Kergaravat et al., 2016).

In this article, we investigate what we can learn about the development of minibasins during coeval shortening from an observation-driven approach based on extensive fieldwork in the Sivas Basin, including regional and detailed structural mapping. The aim of this paper is to propose a mechanism that explains the evolution of Sivas secondary minibasins and salt structures. We describe in detail the surface and sub-surface geometries of the Oligo-Miocene minibasins and investigate the effects of both halokinesis and the tectonic setting. We develop a new tectono-stratigraphic model for the evolution of the Sivas minibasin province, and provide a better understanding of the interaction between halokinesis and regional tectonics on the minibasin development. We discuss the influence of synchronous shortening during salt tectonic activity on (i) the size and shape of the minibasins, (ii) the stratal architecture within the minibasin, and finally (iii) their tilting and rotation.

2. GEOLOGICAL SETTING

The Sivas Basin is an intramontane basin situated at the junction between three crustal blocks: the Pontides magmatic arc to the north, the Kırşehir continental block to the west, and the Taurides-Anatolides continental blocks to the south (Fig. 1A) (Cater et al., 1991 ; Yılmaz and Yılmaz, 2006). The northern and southern margins of the Basin are defined by two suture zones: the Izmir-Ankara-Erzincan suture zone (IAESZ) to the north and the Inner-Tauride suture zone (ITSZ) to the south (Fig 1A) (e.g. Görür et al., 1998; Okay et al., 2006; Yılmaz

and Yılmaz, 2006; Rolland et al., 2010; Karaoğlan et al., 2013). The Sivas Basin overlies the Kirşehir and Taurus blocks and the obducted ophiolite produced by the Northern Tethys closure (Görür et al., 1998; Okay et al., 2006; Yılmaz and Yılmaz, 2006; Rolland et al., 2010).

2.1.From obduction to foreland basin (Maastrichtian – Eocene)

During the Upper Cretaceous to Paleocene a carbonate platform was deposited directly above the ophiolite nappe along the south margin of the Basin (Tecer and Gurlevik Fms; Fig 1B and 2) (Kurtman, 1973; Cater et al., 1991). Following the Sivas Basin basement assemblage, the foreland basin developed during the Early Eocene (e.g. Kurtman, 1973; Cater et al., 1991 ; Guezou et al., 1996; Poisson et al., 1996; Görür et al., 1998). The onset of contraction is recorded by the development of very coarse conglomerates with clasts of ophiolite and limestone derived from the growing topography of the Tecer and Gürlevik platforms covering the active basin southern edge (Fig. 1B and 2) (e.g. Kurtman, 1973; Cater et al., 1991; Poisson et al., 1996). In the south, this conglomeratic fan delta comprises the Bahçecik Fm and is covered by volcanoclastic turbidites of the Bözbel Fm passing laterally to the Kösedağ Fm in the North (Fig. 2) (e.g. Artan and Sestini, 1971; Kurtman, 1973; Özçelik and Altunsoy, 1996). The foreland basin recorded significant shortening in several major pulses of thrusting and folding and depocenter migration toward north from Early Eocene to Pliocene associated with northward Arabian convergence (e.g. Kurtman, 1973; Cater et al., 1991; Guezou et al., 1996; Kergaravat et al., 2016).

2.2.Sivas salt basin

2.2.1. Autochthonous salt and primary minibasins

At the end of the Eocene, the autochthonous salt level, known as the Tuzhisar Fm, was deposited throughout the basin, overlaying the Bözbel Fm and the ophiolite on the southern

basin margin (Fig. 2) (e.g. Artan and Sestini, 1971; Kurtman, 1973; Özçelik and Altunsoy, 1996; Poisson et al., 2010). At outcrop this marine evaporite level comprises interbedded gypsum and anhydrite associated with red silt but it may initially have contained a huge amount of halite (Gündogan et al., 2005; Onal et al., 2008), as evidenced by the important salt related features (e.g. Ringenbach et al., 2013; Callot et al., 2014; Ribes et al., 2015; Kergaravat et al., 2016). Geochemical analysis of the Tuzhisar Fm sulfates demonstrated a Bartonian age from the Sr isotopic ratio (Pichat et al., Submitted). Major continental clastic and playa lake sediments, known as the Selimiye Fm (e.g. Kurtman, 1973; Cater et al., 1991; Gündogan et al.; Onal et al., 2008), progressively covered the autochthonous evaporite level during the Oligocene. The prograding sedimentary loading forced the evaporite to flow basinward, initiating the primary minibasins characterized, to the south of the minibasins province, by a large asymmetric sediment wedge with monoclinal dips and podlike basins with large halokinetic wedges farther north (Fig. 3A) (Kergaravat et al., 2016). The development of the canopy above these primary minibasins in the central part of the Sivas Basin was most probably controlled by the load of the primary minibasins, a decrease of sedimentary supply at the end of the Selimiye Fm, and a likely propagation of shortening northward, inducing the squeezing of preexisting diapirs and walls between the primary minibasins (Kergaravat et al., 2016).

2.2.2. Secondary minibasin generation

In the central part of the Sivas Basin, the secondary minibasins developed above the canopy are filled at their base by (i) a thick succession of fluvio-lacustrine deposits (Karayün Fm), (ii) then the deposition of the shallow marine Karacaören Fm, and finally (iii) the overlying Benlikaya Fm characterized by alluvial to fluvial deposits (Figs. 2 and 3) (Ribes et al., 2015;

153 Ribes et al., 2016). These three formations, forming the minibasins above the salt canopy, are
154 significantly affected by salt tectonics and are the subject of this study.

155 The Karayün Fm, reaching a maximum cumulative thickness of 2 400 m, records the
156 fluvio-lacustrine sedimentation in the Oligocene (Poisson et al., 2010). Three long-lived
157 depositional systems have been recognised from base to top of the Karayün Fm: (1) the Lower
158 member corresponding to playa-lake and distal terminal splay deposits with sedimentary
159 facies similar to the Selimiye Fm deposits; (2) the Middle member corresponding to fluvial
160 braided deposits, and (3) the Upper member corresponding to saline lacustrine deposits (Fig.
161 2) (Ribes et al., 2015). These three depositional systems comprise large-scale genetically
162 related stratal packages that are separated by basin-wide surfaces expressed by changes in
163 textures and facies assemblages, as well as stratal and stacking patterns (Fig. 3). The
164 depositional setting of the Karayün Fm is interpreted as a Distributive Fluvial System (DFS)
165 (Ribes et al., 2015).

166 Above the Karayün Fm, the deposition of the shallow marine Karacaören Fm marks a
167 regional transgression during the Oligocene-Miocene (Özcan et al., 2009 ; Poisson et al.,
168 2010; Sirel et al., 2013; Poisson et al., 2015). The Karacaören Fm contains shallow-marine
169 marls and sandstones that are interbedded locally with algal limestones (Fig. 3) (Kurtman,
170 1973; Özcan et al., 2009; Poisson et al., 2010; Sirel et al., 2013). The Karacaören Fm is
171 divided in two main sub-environments: (i) mixed deltaic and carbonate ramp and (ii) coastal
172 plain and restricted lagoon (Ribes et al., Submitted). At the regional scale, the Karacaören Fm
173 includes two extensive deepening or shallowing-upward cycles which correspond to two
174 major transgressive-regressive sequences (Ribes et al., Submitted).

175 The overlying Benlikaya Fm is characterized by alluvial to fluvial deposits of Middle to
176 late Miocene age, composed of reddish sandstone and conglomerate interbedded with
177 floodplain mudstones (Fig. 2 and 3) (Poisson et al., 1996; Poisson et al., 2010; Ribes et al.,

178 Submitted). The depositional system of this formation is interpreted again as a distributive
179 fluvial system with alluvial/fluvial and playa-lake sub-environments. The Benlikaya Fm
180 overlies a regional erosional surface attributed to a sequence boundary that marks the sudden
181 regional development of a coarse clastic wedge. The overall fining-upward sequence
182 comprises an early aggrading phase (i.e Unit 1, Fig. 2), characterized by widespread coarse
183 deposits in multi-storey channel networks, followed by a retrogradational phase showing a
184 transition towards alluvial plain and playa lake deposits (i.e Unit 2, Fig. 2) (Ribes et al.,
185 Submitted). Toward the Middle of the Miocene, major shortening throughout the southern and
186 central part of the basin marks the end of life of the basin as a depocentre, associated with
187 regional uplift which has continued to the present day (Cater et al., 1991; Guezou et al., 1996;
188 Temiz et al., 2000).

189 ## 3. DATA AND METHOD

190

191 This study is mainly based on remote sensing mapping and fieldwork data obtained during 6
192 months of ground-based work in the central Sivas Basin, using previous maps of Poisson et
193 al. 1996. Remote sensing mapping is based on analyses of very high resolution of colour
194 composite and orthorectified images from the Geoeye satellite (0.5 m resolution) and derived
195 digital elevation models (DEM) with a spot resolution of 2m x 2m. Fieldworks across at least
196 15 mini-basins have been performed to control remote sensing mapping analyses and to
197 measure onto outcrop systematic structural (bedding attitude, fracture and fault planes with
198 slickensides plotted on stereonets), sedimentological and lithostratigraphic data (more than 12
199 km of vertical sedimentological sections were measured, see Ribes et al., 2016). Detailled
200 mapping of minibasins margins have been performed using panorama view highlighting
201 stratal attitude and field mapping of salt-sediment contact and unconformities. Samples have

been collected for facies, anisotropy of magnetic susceptibility (AMS) (Kergaravat, 2016), diagenetic (Pichat et al., 2016) and biostratigraphy analyses (Ribes et al., 2016).

Geological observations and measurements for the present study were compiled onto: (1) a geology map of the minibasins covering an area of 50 × 30 km and finer-scale field maps (at about 1/10,000) of the minibasin contacts and (2) a map of the main structures of the minibasin organized by age, showing internal as well as boundary contacts. Cross sections are based on the surface data, unpublished 2-D seismic lines acquired in 2010–2011 (provided by Transatlantic Petroleum Ltd) and a structural model that we derived from a seismic line published in Kergaravat et al., (2016).

4. STRATAL RECORD OF HALOKINESIS AND SHORTENING

The characterization of the minibasins province relies on the description of several structural and sedimentary features including: (i) the size and the shape of the minibasins (i.e. polygonal or linear), (ii) the stratal architecture related to salt withdrawal (i.e. Wedge and Hook halokinetic sequences and megaflap, see Giles and Rowan (2012) and Rowan et al., (2016)) and the recognition of markers of the regional deformation (i.e. network of either compressional, extensional and/or transfer-fault systems) during the minibasin development. In this section, we analyze the halokinetic and tectonic setting markers through time, from Oligocene to Miocene, in order to highlight the controlling factors of the minibasin development. These markers are summarized on the main structure map (Fig. 4).

We refer to end-member Hook-type Halokinetic Sequence (HHS) and Wedge-type Halokinetic Sequence (WHS), which are characterized by the vertical stacking of drape-folded upturned strata along the edges of diapirs (Giles and Lawton, 2002; Rowan et al.,

2003; Giles and Rowan, 2012). These unconformity-bounded sequences are formed in response to variations in sediment accumulation rate vs. diapir-rise rate (Giles and Lawton, 2002; Giles and Rowan, 2012). Tabular composite halokinetic sequences (TAB), which are formed by stacked HHS, are characterized by drape-folding within 200 m of the diapir and are bounded by unconformities with angular discordance up to 90°. Tapered composite halokinetic sequences (TAP) comprise stacked WHS in which the drape-folding occurs up to 1 km from the diapir, and separated by low angle unconformities up to 30°. We also refer to MegaFlaps (MF), which are defined as "packages of deep minibasin strata that extend far up the sides of diapirs. They are near-vertical but may also be completely overturned in their upper parts, at the transition between feeder diapirs and salt sheets. They occur adjacent to both primary and secondary diapirs and are distinguished from composite halokinetic sequences by their scale, with vertical relief of 2-5 km or more" (Giles and Rowan, 2012; Graham et al., 2012; Callot et al., 2016; Rowan et al., 2016).

4.1.Karayün Fm

The Karayün Fm records the initiation of secondary minibasins above the canopy. This continental formation is mainly exposed in the core of the WABS displaying circular to elliptical geometries that extend for 10 to 25 km² at the surface (Figs. 1B and 3A). These deposits, sub-divided into Lower, Middle and Upper members, display a large variety of salt-related deformation recording various scales of salt-sediment interactions.

4.1.1. Lower member: HHS and WHS

The base of the minibasins expose pronounced thickness variability within and between minibasins with local internal unconformities (Figs. 3A and 4) (e.g. Ribes et al., 2015). Primary sediments above allochthonous evaporite show a characteristic WHS that thins within

a few kms towards the diapir and displays low-angle onlap onto the evaporite such as in the Emirhan and Ilkindi minibasins (Figs. 4, 5A and 5B). These observations show that the allochthonous salt canopy was remobilized almost immediately after the early deposits.

Above the base WHS, sediments continue upward to form successive WHS bounded by internal unconformities with angular discordances of up to 20° (see top-lap on Figs. 5A and 5B). To the East of Emirhan minibasin, the sequences thin over a distance of less than 2 km, from up to 1,000 m in the depocentre to 50 m or less against the eastern evaporite wall, thus forming a TAP (Fig. 5A). This halokinetic wedge succession is partially cut by syn-depositional normal faults dipping both towards the minibasin core and its eastern wall (Fig. 5A). A few meter-scale folds occur that verge toward the minibasin. To the north of the Ilkindi minibasin, this TAP is particularly well exposed, showing a gradual upturning and thinning of beds of the Lower member (Fig. 5B). WHS are limited by internal unconformities toward the Emirhan evaporite weld and defined by southward dips close to 90° decreasing to 30° farther south, over a horizontal distance of up to 300 m (Fig. 5B).

Along other salt structures, such as along the western edge of Emirhan, early WHS can pass upward into a succession of local stratal deformations. Along the evaporite weld which separates the Emirhan minibasin to the east from the Köy minibasin to the west (Figs. 5A and 5C), these deformations consist of 10 to 30 m thick set of strata with little variation in thickness or sand content, which are drape-folded up to a distance of 40 m away from the evaporite weld before becoming parallel to the evaporite weld (Fig. 5C). Each drape-folded sedimentary sequence is cut by an angular unconformity with up to 90° of angular discordance, but becomes conformable within a distance of 50 m from the evaporite weld forming a HHS. Unconformities are mainly connected laterally to reentrants of the evaporite weld, which forms local cusps (Fig. 5C). This vertical succession of HHS, define a TAB, which passes laterally into TAP toward the eastern minibasin margin (Fig. 5A).

4.1.2. Middle member: Megaflap

The Middle member exposes less thickness variability with only basin-scale, halokinetic folds, involving the 300-400 m basal interval, passing upward into wedges along the evaporite structures (Figs. 3A and 4).

Along the eastern Emirhan margin, the lower half of the Middle member comprises a 400 m isopachous sequence of sandstone beds, which is folded over a distance of 1 km from the eastern evaporite wall with bed rotation of up to 90° (Fig. 5A). This sequence is bounded by the evaporite wall with a 90°angular discordance, defining a megaflap. The upper half of this Middle member thins gently eastwards from 700 m in the west to 600 m in the east (Fig. 5A). Rather than being truncated by the basal Karacaören unconformity, the end of the Middle member probably corresponds to WHS.

In the Karayün minibasin, the base of the Middle member is sub-isopachous, while the upper two thirds of it form WHS separated by unconformities, defining a TAP to the eastern margin of the minibasin (Fig. 6). The western extremity of the Middle member displays bed rotations of up to 80° compared to the minibasin center which is truncated by an unconformity of up to 10° and covered by the Upper member (Fig. 6). Numerous syn-sedimentary normal faults cut the tip of the Middle member, dipping both towards the minibasin centre and toward the western Karayün wall and weld (Fig. 6). The eastern margin of the Karayün minibasin displays the deep strata of the Lower member and of the base of the Middle member that extend 5km along the edge of the western evaporite wall. This wall separates the Karayün and Akpinar minibasins, with vertical to slightly overturned beds compared to the center of the Karayün minibasin, thus forming a megaflap (Figs. 6 and 7A) (Rowan et al., 2016). The Middle member lower beds forming the megaflap show few apparent channel migrations, instead comprising both laterally and vertically amalgamated

channelized unit (Fig. 7A) (Ribes et al., 2016). The extremity of the Karayün megaflap is a complex structure showing a refolded tip of the megaflap limb, which is truncated and overlain by the Karacaören Fm to the west and by a complexly interbedded gypsum and shale horizon to the east (Figs. 7B and 7C). The eastern end of the Middle member section corresponds to a tilted, faulted and recumbent fold with a right-lateral strike-slip fault (Figs. 7B and 7C).

Along the western margin of the Karayun minibasin, the Lower and Middle members are locally cut by a northeast-verging thrust fault connected to the evaporite wall between the Arpayazı minibasin to the north and the Ilkindi minibasin to the south (Fig. 6). The westernmost end of the Karayün evaporite wall, separating the Ilkindi and Arpayazi minibasins, disappears buried beneath a small E-W trending anticline, the northern flank of which is cut by a thrust fault verging north (Fig. 6). On the northern side of the north-verging thrust fault, beds of the Middle member display a set of asymmetrical folds with axial planes dipping toward the south (Fig. 6). This large-scale structure defines a thrusted evaporite-cored anticline, whose northern flank is cut by a north-verging thrust fault, emplacing the anticline core on top of the Arpayazı beds (Fig. 6).

4.1.3. Upper member: WHS and encapsulated minibasins

The Upper member is observed above both preexisting minibasin and allochthonous evaporites. At outcrop, the overall thickness of the member is highly variable due to large-scale WHS (Fig. 4).

In the Karayün minibasin, the entire Upper member displays a large stratigraphic wedging that extends on both sides with vertical to slightly overturned beds compared to the minibasin center (Fig. 6). Along the western minibasin margin, the wedge involving the Upper member shows a drape-fold geometry affecting a wide zone of 500–1 000 m from the Karayün weld,

with bed rotations of up to 110° from the minibasin center (Fig. 6). This halokinetic drape-fold upper boundary is a 90° angular discordance that becomes conformable within up to 1 km from the Karayün weld (Fig. 6). To the eastern margin of the Karayün minibasin, a large sedimentary wedging, involving the entire Upper member, also displays a drape-fold geometry affecting a zone up to 1000m wide with bed rotation of up to 100° from the minibasin center. In a way similar to the western margin, an erosional unconformity cuts the lip of the wedge but with lower angular discordance (50-60°) preserving a larger part of the limb of the wedge and covering the Karayün megaflap than in the west (Fig. 6).

Four small-scale minibasins, composed exclusively of the Upper member of the Karayün Fm (i.e. Pınarca, Köy, Inceyol and Ulukapı) west of the Emirhan minibasin, have circular to elliptical shapes defined by synclines covering allochthonous evaporite (Fig. 5A). One of these minibasins, the Inceyol minibasin is composed of a single syncline in the north, which passes laterally into two tight synclines to the south (Fig. 8A, see Collon et al., (2016)). These two synclines are separated by an exposed evaporite wall, interpreted at depth as a weld or a narrow evaporite wall juxtaposing steep to overturned flanking strata on both sides (Figs. 8B and 8C). Along the western flank of the eastern syncline, the beds display apparent onlaps on the evaporite wall with overturned strata dipping 55°W passing to vertical attitude over a distance of 50 m in the core of the syncline (Fig. 8A). Strata in the two synclines are cut by numerous normal faults, and local reverse faults are also observed in the core of the eastern syncline. Due to the overturned strata along the evaporite-flanked wall, the isolated tight synclines forming the Inceyol minibasin define an encased minibasin sensu Pilcher et al., (2011), also known as an encapsulated minibasin sensu Rowan and Inman (2011).

4.2.Karacaören Fm

The Karacaören Fm fills minibasins that extend 10 to 30 km² at the surface, displaying elongated geometry with roughly NE-SW trends (Fig. 3A). This shallow marine deposit

overlays both preexisting primary and secondary minibasins either limited by an angular unconformity or lying directly above the canopy (Fig. 3B).

4.2.1. Base of the Karacaören Fm

A major unconformity is observed in the minibasin province at the base of the Karacaören Fm, cutting down to variable stratigraphic depths on different structures (Fig. 4). For example, in the Celallı anticline, this erosive unconformity separates the Selimiye Fm. from the Karacaören Fm, with high-angle (up to 90°) unconformities between the marine Karacaören beds and the Selimiye Fm folded beds (Fig. 9A, location Fig. 4) (e.g.Cater et al., 1991). A second example of the major marine unconformity is present between the Karayün and the Karacaören formations, characterized by high-angle unconformities along minibasin margins within the Emirhan and Karayün minibasins (Fig. 9B, location Figs. 4 and 5A).

4.2.2. Stratal architecture

Along the western margin of the Karayün minibasin, above the marine unconformity, the base of the Karacaören Fm presents a stratigraphic wedge which thins over a distance of 400 m from the Karayün evaporite weld, and is bounded by angular discordances of up to 15° forming a TAP (Fig. 6). To the west of the Akpınar minibasin, the basal beds consists of a marine conglomerate preserved as an eroded TAP to the SE above the evaporite diapir, and as a syncline above the mixed gypsum and shale complex (Fig. 7C). Above the basal marine TAP, the marine shale and sandstones record a succession of stratigraphic wedges which progressively onlap the mixed gypsum and shale as well as the marine conglomerate syncline, over a thickness of 400 m, recording successive steps of the salt withdrawal (Fig. 7C). The Karayün megaflap and the tapered CHS at the Akpinar minibasin base are both overlapped by the Middle to Upper Karacaören Fm.

The Karacaören formation is also exposed as broad stratigraphic wedges extending up to 2000 m away from the evaporite structures (Fig. 4). These halokinetic wedges are observed in

several minibasins (i.e. Akpınar, Tuzhisar, Bingöl, Emirhan and Ağılkaya) and are both N-S and E-W trending.

In the Tuzhisar minibasin, large stratigraphic wedges are observed in map view thinning towards both the eastern and western minibasin margins where an unconformity cuts the halokinetic wedge limb at an angle ranging between 40 and 50° (Figs. 3A and 4). Two large stratigraphic wedges thin toward the center of the Tuzhisar minibasin over 3 km, where the limbs are cut by numerous syn-sedimentary normal faults (Fig. 3A). These stratigraphic wedges are also observed in panorama view with N-S trending beds thinning towards the south over a zone more than 2000m wide (Fig 10A, location Fig. 4). Farther south, the Ağılkaya minibasin is composed of two synclines showing vertical to overturned flanks, bounded by a central anticline which passes westward to an evaporite wall (Fig. 10B, location Fig. 4). These synclines expose asymmetrical wedges on both flanks, thickening towards the fold axes with progressive bed rotation (Fig. 10B). The northern flanks also show wedges of sediments that thin out over a shorter distance than along the southern flank (Fig. 10B). The same type of halokinetic growth strata is observed in the Bingöl and Çaygören minibasins (Fig. 4). Numerous syn-sedimentary normal faults cutting the base or the Middle part of the Karacaören Formation are observed, mainly in minibasins emplaced directly above the allochthonous evaporites, for instance in the Tuzhisar and Ağılkaya minibasins (Fig. 4).

4.3.Benlikaya Fm

The Benlikaya Fm is exposed mainly at the rim of the minibasin province (Fig. 3A). These deposits display moderate thickness variations compared to the Karayün and Karacaören formations (Fig. 4). Some large stratigraphic wedges are localized at the front of regional thrusts passing through the NE-SW salt wall and few local WHS are observed to the north of the minibasin province (see the eastern margin of the Kizilkavraz minibasin in Fig. 4).

Locally, traces of allochthonous salt are observed, such as in the Çaygören minibasin and around the Kabali Diapir (Fig. 4). This continental sequence is deposited both above preexisting secondary minibasins such as the Çaygören minibasin, and allochthonous evaporite such as the Küpecik minibasin (Fig. 3A).

4.3.1. Thrust faults systems

The eastern part of the minibasins area is characterized by major, sub-parallel N70E, striking thrust faults passing through evaporite walls, delimiting elongated minibasins with a regular spacing of 4 to 6 km (Fig. 4). Some of these thrusts were previously described and named by Temiz (1996). All the thrusts are south verging, parallel to the regional fold trend, and associated with blocks of serpentinized peridotites (Figs. 4 and 11) (e.g. Cater et al., 1991). From south to north, these tectonic structures are referred to as the Celallı (CT), Gölcük (GT) and Tuzhisar (TT) thrusts, connected to the Karayün Transfer Zone (KTZ) to the west. The Gölcük thrust (GT) is considered to be one of the major thrusts within the secondary minibasin domain, separating the Karayün and Akpınar minibasins to the NW, from the Celallı anticline to the SE (Fig. 11, location Fig. 4). The GT footwall is characterized by a growth syncline, involving the Benlikaya Fm., affected by south-verging satellite thrust faults (Fig. 11). The GT contains blocks of serpentinized peridotite, some of which are 100m in size. These ultramafic blocks, also observed below and within the autochthonous evaporite horizon, are interpreted as olistoliths and debris flow deposits derived from the uplifted southern margin of the Basin, emplaced before and during deposition of the autochthonous salt (Fig. 1A). We suggest that these blocks were later transported upward by the flowing evaporite during diapirism, squeezing of the evaporite wall, and finally emergence of the thrust.

4.3.2. Strike-slip faults systems

Several strike-slip fault zones are observed along the KTZ in Fig. 4 and the associated stereo plot in Fig. 12. The first of strike-slip fault zone is located between the Emirhan, Eğribucak and Karayün minibasins (Fig. 6, location 1). Along the evaporite weld separating the Eğribucak and Karayün minibasins, beds are cut by N130 right-lateral strike-slip faults with a few meters of offset (Figs. 6 and 12). Fault planes are distributed en-echelon and left-stepping with lengths of about 100 m, defining the weld as a wrench weld between the Eğribucak and Karayün minibasins (Fig. 6, location 1). Farther west in the Karayün minibasin, the upper Karacaören beds are cut by a synthetic strike-slip, en-echelon fault array, with a dextral offset of several tens of meters as well as left-stepping faults (Figs. 6 and 12, location 2). Fault plane traces trending N130 are connected to the evaporite wall and extend over a length of 1 km (Fig. 6).

The second strike-slip fault array along the KTZ is located between the Arpayazı and Karayün minibasins (Fig. 6, location 3). To the north of the Arpayazı minibasin, at the wrenched weld contact, the Karayün Fm is cut by strike-slip faults with dextral displacement along the KTZ between the two minibasins (Figs. 6 and 12). To the northeast of the Arpayazı minibasin, numerous N150 trending faults with traces extending over a few hundred meters cut the minibasin edges, where the evaporite wall grades into a wrench weld with dextral motion (Fig. 6, location 3). The present-day distribution of these faults at the base of the Arpayazı minibasin suggests that these structures could initially have been normal faults, reactivated after the rotation of the minibasin as synthetic strike-slip faults with a dextral offset, assisted by the presence of gypsum. However, most of the syn-sedimentary normal faults observed in other minibasins associated with stratigraphic wedge development (i.e. west Karayün minibasin, Fig. 6) verge toward the centers of the minibasins, which is not the case

for the faults situated at the base of a large stratigraphic wedge truncated to the north-east of the Arpayazi minibasin (Fig. 6).

Another example of a strike-slip fault zone is the wrench weld bounding the Emirhan minibasin to the north and the Ilkindi minibasin to the south, i.e. the Emirhan weld (Fig 5A, location 4). Synthetic strike-slip faults trending N80 and N120, with a dextral offset and fault traces of a few hundred meters, are connected to the wrench weld and cut beds of the Karayün Fm (Figs 5A and 12). Antithetic strike-slip faults with sinistral offsets are also observed with a N160 trend (Fig. 12). These fault structures record a dextral component of displacement for the wrench weld between the Emirhan and Ilkindi minibasins.

To the north of the Emirhan minibasin, two other faults, with sinistral offset, trend N30-N60 and merge along-strike within the E-W evaporite wall, with 500-m-long fault traces. Both cut the base of the Eğribucak and the top of the Emirhan minibasins (Fig. 5A and 12, location 5). The two faults delimit an evaporite wall segment, which shows an apparent clockwise rotation around vertical axes recording a dextral component of displacement between Emirhan and Eğribucak minibasins (Fig 5A).

Strike-slip fault zones are also observed affecting the cores of minibasins. Along the western edge of the Arpayazi minibasin (Fig. 6, location 6), numerous en-echelon strike-slip faults cut through the entire minibasin, with right-stepping faults showing sinistral offsets of a few meters (Fig. 12). This cluster of strike-slip faults is probably conjugated with the Karayün Transfer Zone (KTZ) that shows a dextral offset to the east (Fig. 6).

Fault zones can also be observed along thick evaporite walls. Along the N-S evaporite wall separating the Ilkindi minibasin from the Eskiboğazkesen minibasin to the west, the southwestern part of the Ilkindi minibasin shows a left-lateral strike-slip fault cutting beds of the lower and Middle member (Fig. 4, location 7). The fault is NW-SE trending and 1.5 km

long. This fault is linked to the N-S evaporite wall to the north, and to the secondary weld delimiting the Yavu minibasin to the south, with a large offset, probably greater than 500 m.

4.3.3. Salt sheet

Evidences of an allochthonous salt are found in the Çaygören minibasin, located to the north of the Emirhan minibasin (Figs. 3A and 13). On the northern side of the Çaygören salt wall, the Karacaören and Benlikaya strata form large stratigraphic wedges, showing progressive bed rotation with dips varying continuously from 70° toward the south along the flank of the evaporite wall, to 35° farther north (Figs. 13A and 13B). Within the Benlikaya Fm, an evaporite body, about 600m in width and reaching a thickness of 100m, is present at surface (Fig. 13A). At the base of the evaporite body corresponding to its southern limit at surface, the Benlikaya beds, dipping 80°N, are truncated by a steep evaporite-sediment interface defining an evaporite ramp. Northeast of the evaporite body, the Benlikaya fluvial beds, dipping 80°N and flanking the evaporite body, are concordant with the evaporite-sediment contact, defining a flat contact, with only rare evidence of normal faults within the Benlikaya Fm and no evidence of shear at the salt-sediment contact (Figs. 13A, 13B and 13C, location number 1). Northeast of the flat contact, the Benlikaya beds dipping 35°N and flanking the evaporite body, are truncated with an apparent angular discordance of 30° by an evaporite-sediment interface, again defining a basal ramp (Fig 13A, 13B and 13D, location number 2). This evaporite-sediment ramp contact is characterized by a shear zone, up to 1 m thick, composed of sandstone, gypsum lenses and sandstone boudins displaying clockwise rotation related to a dextral motion (Fig. 13D). The top of the evaporite body, corresponding to its northward outcrop limit, is marked by drape-folds involving Benlikaya strata with rotations of up to 70° and no evidence of thrust faults (Fig. 13B). The Benlikaya beds, overlying and flanking the evaporite body, locally contain normal faults with cm-scale extensional displacements. North-verging recumbent folds associated with shear zones extend tens of

meters within the evaporite body (Fig. 13B). The large-scale isolated evaporite body presenting ramp-flat geometry, is interpreted as remnant of a section across an evaporite sheet limb, emplaced during deposition of the Benlikaya Fm and probably fed by the nearby southern Çaygören evaporite wall, the connection to which has been eroded (Fig. 13B).

5. SECONDARY MINIBASINS STRUCTURES

Three N-S cross-sections passing through the minibasin province illustrate mainly the geometry of secondary minibasins, which are well constrained at the surface but poorly constrained at depth by unpublished seismic lines, due to the presence of both allochthonous and autochthonous salt levels, as well as complex structures along the vertical contacts of the minibasins (Fig. 14, see Fig. 3A for locations). Therefore, several geometries, thicknesses and basement configurations are possible.

Several secondary minibasins, located to the north of the Ilkindi and Karayün minibasins, are tilted up to vertical toward the north (i.e. Emirhan, Eğribucak, Çaygören, Tuzhisar and Karayün minibasins, Figs. 3A and 14). The continental Karayün Fm and the marine Karacaören Fm are characterized by large stratigraphic wedges, which generally thin toward the south in the case of the Karacaören strata, such as in the Tuzhisar minibasin, and by the tightening of synclinal minibasins above the canopy, such as in the Ağılkaya minibasin.

Diapirs rising from the canopy have varying geometries related to various halokinetic sequences along their flanks. Although some diapirs are still preserved, many others with outcropping evaporite walls have been squeezed, forming vertical welds, sometimes evolving to thrusted welds where minibasins are juxtaposed. Teepee-like geometries are observed when strata dip away from the welds in opposite directions (e.g. Rowan and Vendeville, 2006). Section C in the east shows diapirs verging toward the south compared to those on sections A and B where the diapirs are less defined (Fig. 14). The salt geometries change radically laterally, as seen between Ilkindi in the south and Emirhan and Arpayazı in the north, passing from a teepee-like geometry to a thrusted evaporite wall. These salt structures can also display a strike-slip component of movement generated by the translation and rotation of the minibasins about a vertical axis, as shown in the previous section.

6. EVOLUTION OF THE SIVAS SECONDARY MINIBASINS

Based on the previous observations, summarized on the main structure map and cross sections (Figs. 3B, 4 and 14), an evolutionary model of the secondary minibasin generation is proposed. It is illustrated in Fig. 15 by five sequential schematic diagrams, starting in the Mid-Oligocene during the initiation of the minibasins (Lower Karayün Fm), and ending in the Middle Miocene (Benlikaya Fm). The aim of this schematic restoration is to highlight the competition between halokinesis and contractional loading on the minibasins development.

6.1.Secondary minibasins and diapirs initiation (A)

During the sinking of early sedimentary deposits, mainly local composite halokinetic sequences developed along both East-West and North South directions (e.g. Ribes et al., 2015; Ribes et al., 2016). This results in the formation of a polygonal network of salt

anticlines with pillows at their intersection surrounding isolated, subcircular to elliptical basins, filled by lower Karayün beds (Fig. 15a). The topography generated by the salt rise relatively to the sedimentation rate locally controls the sediments dispersal and may facilitate the local chemical and mechanical remobilization of evaporites (e.g. Lawton and Buck, 2006 ; Paz and Rossetti, 2006; Ribes et al., 2016). Syn-sedimentary normal faults, rooted in the basal allochthonous salt, cut edges of the halokinetic wedge sequences. In the case of the secondary minibasin initiation, the salt canopy limits both (1) the controls exerted by the subsalt network of salt structures surrounding primary minibasins (e.g. Diegel et al., 1995; Harrison and Jackson, 2014) and (2) the influence of regional boundary conditions related to the northward propagation of the Sivas foreland fold and thrust belt (e.g. Kergaravat et al., 2016).

The initiation of the secondary minibasins during the deposition of the Lower member is driven mostly by the salt-induced local accommodation, generated by salt withdrawal (e.g. Ribes et al., 2016). Although the random localization of the primary depocenter of the secondary minibasins is still poorly understood, local depressions at the salt canopy surface potentially initiated the primary deposits. Local allochthonous salt depressions may have originated from (1) the heterogeneity of intra-salt deformation between levels of gypsum, anhydrite and halite (e.g. Cartwright et al., 2012; Jackson et al., 2014), (2) local salt collapse within the allochthonous salt due to salt dissolution (e.g. Jackson et al., 2010), and (3) morphology of the salt canopy such as the suture synclines at junctions between salt sheets (e.g. Dooley et al., 2012) (Fig. 15a). In the case of the Sivas basin, where the salt level is composed by halite, gypsum and anhydrite, intra-salt deformation allowed by regional shortening is probably the most efficient way to initiate local topography in the salt canopy.

6.2.Buried diapirs (B)

The Middle member records an abrupt lithological change with the arrival large amount of coarser sediments, with a dominantly northward fluvial transport direction (Ribes et al., 2016). A globally isopachous and homogeneous sedimentary package covers both preexisting depocenter and salt structures, obscuring the preexisting salt topography (Kergaravat et al., 2016; Ribes et al., 2016) (Fig. 15b). Small thickness variations reflect the crests of salt structures showing the weak influence of halokinesis. At the top of preexisting salt structures, syn-sedimentary normal faults, sometimes connected to the evaporite, cut this coarser sedimentary package, recording the local influence of salt withdrawal, which is weak but still active (Fig. 15b).

The abrupt increase of sedimentary rate in the minibasin province is attributed to a regional uplift of the southern margin of the basin, a consequence of a pulse of activity of the orogenic wedge and associated thrusts (Kergaravat et al., 2016) (Fig. 15b). Burial of the salt structures results from a period of regional accommodation induced by foreland flexural subsidence and relative high sedimentation rate (Kergaravat et al., 2016; Ribes et al., 2016). As proposed by Ribes et al., (2016), the relative decrease of salt withdrawal rate could also represent a slightly delayed response to the abrupt and regional sediment loading. In addition, we suggest that the presence of coarser sediments at the top of salt structures, which are more difficult to deform, have probably decreased the vertical flow rate of salt diapirs.

6.3.Rejuvenation of diapirs (C)

The end of deposition of the Middle member is marked by a sharp increase in vertical diapiric flow, associated with large halokinetic folding and even megaflaps development affecting the homogeneous and isopachous Middle member (Fig. 15c). Large halokinetic folds form along both East-West and North-South salt structures (Fig. 15c). Coeval drape folding and wedging

589 of the Upper member strata both illustrate renewed diapir motion related to their squeezing
590 most probably due to the orogenic shortening. High evaporite topographies are produced
591 during halokinetic fold development, and probably fed saline lacustrine deposits of the Upper
592 member by salt walls and diapir crests remobilization. At the top of salt walls and diapir
593 crests, encapsulated minibasins showing large wedging of the Upper member are developed.
594 Their development at the crests of squeezed salt walls is probably favored by (1) local
595 extension at diapir crests during salt diapir squeezing (e.g. Vendeville and Nilsen, 1995;
596 Callot et al., 2007) and (2) early strike-slip motion within the salt wall and diapir producing
597 local pull-apart between minibasins where sediments may be deposited (e.g. Sherkati and
598 Letouzey, 2004). In addition, we suggest that the rejuvenation of salt diapir rise is favored by
599 a decrease of sedimentation rate compared to the diapir growth rate, in particular due to the
600 transition from fluvial sediments of the Middle member with a relatively high sedimentation
601 rate, to the low sedimentation rate of the lacustrine deposits of the Upper member.
602 Encapsulated minibasins, located at diapir crests, are geometrically similar to the pod- like
603 structure incorporated within the ductile layer modeled by Fort and Brun (2004),
604 preferentially formed in domains subjected to shortening. The presence of this intrasalt
605 sediment have probably influence the lateral mobility of minibasins during shorting and the
606 resultant structural style (e.g. Duffy et al., 2017).

607 ### *6.4.East-West elongated marine minibasins and preferential growth of salt*
608 ### *structures (D)*

609 The arrival of the marine transgression is marked by regional erosion affecting high relief
610 areas such as diapir crests where the tips of halokinetic folds expose continental beds (Fig.
611 15d). In contrast to the older minibasins, filled by the Karayün formation, linear minibasins
612 develop elongated at right angles to the regional shortening direction (Fig. 15d). Local
613 halokinetic sequences are mainly developed within the base of the shallow marine sequence.

Most of the minibasins present large stratigraphic wedges which can form "Heel/Toe" geometries, where the marine succession thickens in a direction opposite to that of the early Karayün wedges, highlighting the presence of a basal welding of the basin (Fig. 15d) (e.g. Kluth and DuChene, 2009).

The preferential growth of salt walls and diapirs trending East-West is attributed to the squeeze of preexisting evaporite walls at right angle to the regional N-S shortening which act as thrust faults where minibasins developed. However, the presence of halokinetic wedges along both East-West and North-South salt walls suggest that salt withdrawal related deformation is still effective. Elongated minibasins seems to result from a combination of thrust-top basin subsidence, i.e. piggy-back basin, related to salt walls and diapirs squeezing during thrusting, and local salt withdrawal accomodation.

6.5.Minibasin rotation and tilting (E)

During deposition of the Benlikaya Fm in a peripheral position in the southern and northern minibasin province, the coeval uplift of the central minibasin province is associated with substantial tilting of the minibasins during thrust emergence (Fig. 15e). The squeezing of salt structures leads to the formation of evaporite welds, which are developed both at right angles and oblique to the regional shortening direction (Fig. 15e). As there is little to no evidence of a shift of the minibasin depocenters toward the future salt weld, the shrinkage and welding of the salt walls is attributed to the orogenic shortening transmitted to the minibasins province (e.g. Rowan et al., 2012). At surface, allochthonous evaporite emerges due to strong squeezing of salt structures (Fig. 15e). The fully developed welds in the minibasin province are attributed to wrench welds whereby the layer-parallel translation of wall rock and the associated dissolution enhance salt removal until complete evacuation of the remaining evaporite (e.g. Hudec and Jackson, 2007; Wagner and Jackson, 2011). Strike-slip fault zones affect both entire minibasins and their margins along welded contacts, the origin of which are

related to the various degrees of minibasin translation and rotation about vertical and horizontal axes during orogenic shortening, see section below (Fig. 15e).

7. DISCUSSION

7.1.Impact of shortening on minibasin behavior

The domain of secondary minibasins records in the Sivas Basin the evolution from a basin controlled by salt tectonics to a tectonically controlled basin. To analyze the relative importance of these two main structural controls, several features have been identified as key indicators, among them the size and shape of the minibasins, their stratal architecture and their tilting and rotation.

We propose that the recognition and analyses of these markers can be used to discriminate between a mainly salt-controlled and a mainly shortening-controlled system with a range of possibilities in between (Fig. 16).

- For the salt dominated/controlled system, the minibasins are mainly sub-circulars surrounded by large salt walls and diapirs. There is a high variation in thickness within and between minibasins, and local halokinetic sequence shapes and dimensions (both wedges and hooks structures) vary from one side of the minibasin to the other (Fig. 16A).
- For the compressive dominated system, the minibasin shapes evolve from subcircular to elongated (i.e. dominated by thrusting and thrust top basin development) (Fig. 16B). The pre-existing minibasins record major tilting and

rotation about vertical axis, accommodated by strike slip fault zone along the margins, large thrust faults at right angle to the regional shortening, rooted in the salt walls and complete welding of salt structures are observed (Fig. 16C).

- Between these two end-members, the initial architecture of salt controlled minibasins and the salt structures network are more and more affected by the regional shortening through time and may be characterized by the progressive development of halokinetic folds, megaflaps, allochthonous salt stocks emplacements, and tilting of minibasin.

The effect of orogenic shortening on minibasin evolution is clearly dependent on the available salt stock for minibasin accommodation (i.e. salt level thickness). The coupling of the salt related minibasin deformation to the regional tectonic setting initiated when the salt horizon thinned such that there was not enough to decouple deformation.

7.2.Impact of salt structures pattern on shortening style

The previous sections present the rotation about vertical axes as well as the translation of minibasins, accommodated by strike slip faults zone along minibasin edges during diapir squeezing (see Fig. 15F). A similar situation is observed on passive margins with rotation of blocks during sediment gravitational gliding/spreading, accommodated laterally by strike-slip shear (e.g. Fort et al., 2004). In the case of the Angolan margin, rotation of block about vertical axis started early and the cause of rotation is attributed to a differential sedimentary load above salt during rafting of block (e.g. Fort et al., 2004). In our study, there is no clear evidence of minibasin rotation about vertical axis during downbuilding of the minibasins (i.e. depocenter migration toward salt weld). The gravity-driven processes (i.e. gliding and spreading) seem to have minor effect, contrary to the regional shortening influence that is

preferentially accommodated by squeezing of salt structures (e.g. Kergaravat et al., 2016). Given homogenous regional shortening, what is the origin of minibasins rotations about vertical axes?

In map view, the structural pattern of the secondary minibasins changes form West to East limited by the KTZ (Fig. 4). In the West, salt walls and welds with NE to NW directions separated sub-circular minibasins and encapsulated minibasins, whereas in the east, sub-parallel N70E salt walls separated dominantly linear minibasins. The KTZ, a major strike-slip fault zones with senestral motion is developed at minibasin margins, and evidences a variation of minibasins lateral mobility (Fig. 16C). We suggest that in case of the Sivas Basin, the main factor controlling the minibasin lateral mobility is the differences in width and orientation of the pre-existing complex 3D structure of the evaporite wall network, compared to the regional shortening direction (Fig. 16C). The various amount of minibasins lateral displacement encourage the rotation about vertical axes of the minibasins (Fig. 16C). The minibasin rotation is recorded by strike-slip fault zones located at minibasin margins and particularly along salt structures that are at high angle to the regional shortening direction (i.e. the salt-sediment contact between Arpayazi and Karayun minibasins).

7.3. Origin of the minibasin tilts

Considering the rotations about horizontal axes, or tilting, the rotation of the minibasins appears systematically oriented toward the north (e.g. Emirhan and Karayün minibasins, Fig. 14). Tilting of minibasins up to 90° rotation suggests a significant amount of shortening. However, part of the tilting may result from the downbuilding of the minibasin and depotcenter migration due to basal salt flow associated with halokinetic wedging (e.g. Hudec et al., 2009). This process is in particular evidenced by the important contrast between the

apparent high stratigraphic cumulated thicknesses (up to several kilometers) and the poor maturity recorded in the rocks. Available maturity data suggest that the Karayun levels are still immature to very low maturity, indicating a limited amount of minibasin burial (Tmax of 430°C to 440°C, %Ro<0.7, i.e. less than 3km; (Huvaz, 2009 ; Erik et al., 2015)). This burial is much lower than the recorded cumulative stratigraphic thickness, and this suggest that this thickness may be only apparent and overestimating the real accommodation. Differential downbuilding, such as Heel-Toe geometries, may explain this discrepancy, evidencing thus a progressive rotation of the basins during their development. But such process cannot generally explain complete 90° tilt of a minibasin, thus in case of the Sivas basin, several processes are advocated to explain the tilting of minibasins (Fig. 17):

(1) The advance of the fold and thrust belt underneath the minibasins is accommodated by the formation of thrust sheets (Fig. 3B). This development of subsalt, south verging thrust sheets, resulted in the rise and the rotation of the minibasins located: (i) at leading edge of the thrust sheet that pushes the minibasin against a welded minibasin acting as a stopper, i.e. Ilkindi minibasin at front of tilted Emirhan minibasin or else (ii) at the leading edge of the thrust sheet uplifting the minibasin along a backthrust acting as a triangular zone (Figs. 3B and 17A).

(2) The development of the southern tectonic wedge to accommodate the regional compression induces a tilt of the foreland toward the south (Fig. 3B) (see Kergaravat et al., 2016). The subsalt tilting may induce the gliding of the minibasins toward the center of the Wall and Basin domain (Fig. 17B). In a way similar to the toe of passive margins, where the shortening domain develops in the distal part of the slope, thrust fault passing through salt structure have transported minibasins against a welded minibasin acting as a stopper (Fig. 17B) (e.g. Fort et al., 2004).

(3) The heterogeneity of the domain located below the canopy, including primary minibasins and early salt feeders results in a pre-canopy basal topography. Formation of early basal welds at the periphery of the minibasins domain induces a rotation toward the thicker salt central domain (Fig. 17C). A similar process is described in the Paradox Basin where the presence of an asymetric basal weld induces a rotation of the minibasin forming a 'Heel-Toe structure' (e.g. Kluth and DuChene, 2009).

Tilting of minibasins up to 90° have not been observed at the toe of passive margins where gravity gliding and spreading is the main cause of shortening. We suggest that the association of (1) depocenter migration, i.e. stratigraphic wedging due to basal salt escape, and (2) formation of thrust sheets are the dominant process in the Sivas basin allowing for the strong tilting of some minibasins.

8. CONCLUSION

The central Sivas basin provides a spectacular example of a minibasin province developed above an evaporite canopy, and offers a rare opportunity to study the interaction between regional shortening and halokinesis. We have shown that the Oligo-Miocene period is characterized by an increasing number of shortening evidences, and a correlative decrease of the local halokinesis imprint, within the minibasin province. The major results of the general tectono-stratigraphic framework of the Sivas minibasin evolution are listed below.

- The initiation of the Sivas secondary minibasins is driven mostly by the salt-induced local accommodation forming a polygonal network of salt structures surrounding isolated, sub-circular to elliptical depocenters, with mainly local

758 composite halokinetic sequences developed all along the margins of the
759 minibasins.
760 • The relative abrupt increase of sediment deposition rate, compared to salt
761 withdrawal, is attributed to the advance of the orogenic wedge toward the
762 minibasin province. This period of tectonically controlled regional
763 accommodation, induced by flexural foreland accommodation, results in the burial
764 of the preexisting salt structures.
765 • Orogenic compression encourages a rejuvenation of salt structures marked by a
766 sharp increase in vertical diapiric flow, producing large post-depositional
767 halokinetic folds such as megaflap.
768 • The network of salt structures evolved from a polygonal to a linear pattern,
769 oriented at right angles to the regional shortening direction. Shortening leads to the
770 squeezing of salt structures forming welds, which developed both at right angle
771 and in oblique position compared to the regional shortening direction.
772 • The importance of composite halokinetic sequences decreases trough time, and
773 large stratigraphic wedges become the dominant salt-related structures.
774 • The orogenic shortening is clearly recorded during the end of the secondary
775 minibasin province evolution, associated to emergences of thrust faults and
776 squeezing of salt structures causing emplacement of the salt sheet. This period
777 seems to correspond when allochthonous salt became thinner and insufficient to
778 efficiently decouple surface deformation from the orogenic shortening.
779 • The pre-existing complex 3D structure of the evaporite wall network compared to
780 the regional shortening direction influences the lateral mobility of the minibasins
781 and the resultant structural style of the minibasin province. Minibasins are both

tilted and rotated about vertical axes in response to the formation of strike slip fault zones.

The shortening has a major influence during the evolution of a minibasin province, the importance of which increases with the expulsion of the salt.

9. ACKNOWLEDGEMENTS

We thank Total SA for their financial contribution. The fieldwork data in this study have been acquired in collaboration with the Cümhuriyet University in the name of Haluk Temiz and Kaan Sevki Kavak, and we would like to thank them for their help and support during the fieldwork. Special thanks are due to J. Letouzey, M.P.A. Jackson, M. Hudec, A. Poisson, B. Vrielynck, and J.F. Salel for fruitful discussions in the field. We are grateful to P. Crumeyrolle, C. Bonnel, E.Legeay, A. Pichat and G. Hoareau for their contributions in understanding the region and field work participation.

10.FIGURE CAPTIONS

Fig. 1. (A) Tectonic setting of Turkey, showing main continental blocks, Oligo-Miocene Sivas basin deposits, outcrops of ophiolites, and ophiolitic mélanges belonging to the Tethyan realm and major suture zones including the Izmir-Ankara-Erzincan suture zone (IAESZ), the Inner-Tauride suture zone (ITSZ), the Bitlis-Zagros suture zone (BZSZ), and Oligocene-Miocene deposits of the Sivas Basin after Okay (2006), Stampfli (2000) and Karaoğlan (2013). (B) Map of the distribution of evaporite outcrops at the Sivas Basin scale and Oligocene-Miocene deposits with main thrusts and back thrust faults and folds axes, location of study area corresponding to geological map (Fig. 4A), after Kergaravat (2016)

Fig. 2. Composite regional lithostratigraphic column showing depositional environments, formations, average thicknesses of the various stratigraphic units in the central Sivas Basin and tectonic events of the Central Sivas Basin (modified after Kurtman, 1973; Çiner et al., 2002; Ribes et al., 2015; Kergaravat et al., 2016). Light grey box shows relevant stratigraphy to this study.

Fig. 3. (A) Geological map of the central Sivas Basin corresponding to the secondary minibasins domain with position of cross sections and geological maps of minibasins margins (see Fig. 2 for location), after Kergaravat (2016) and modified after Poisson (1996). (B) North-South cross section through the center of the Sivas Basin based on seismic line and surface data showing, from south to north the subsalt tectonic wedge of Paleocene-Eocene beneath the autochthonous evaporite, a large asymmetric minibasin belonging to the first generation of minibasins, the second generation of Oligo-Miocene minibasins above an evaporite canopy exposed in the central Sivas basin, and the flat northern widespread evaporitic domain, after Kergaravat (2016).

Fig. 4. Map of structural elements and the distribution of evaporite outcrops at the WAB domain scale (same location as Fig. 3A) showing traces of salt weld, ultramafic blocks and fold axis. The age of the trace of thrusts, extensional and strike-slip faults, Hook (HS) and Wedge (WS) halokinetic sequences, Tabular and Tapered composite halokinetic sequences in orange correspond to the deposition of the Karayün Fm (Oligocene), in blue to the deposition of the Karacaören Fm (Late Oligocene-Early Miocene) and in red to the deposition of the Benlikaya deposition (Middle-Late Miocene).

Fig. 5. (A) Detailed geological map of the tilted Emirhan minibasin surrounded by the Inceyol, Ulukapı, Köy, Pinarka, Eğribuçak, Arpayazi and Ilkindi minibasins with the location of the composite halokinetic sequences, halokinetic folds, trace of unconformities, welds, strike-slip and syn-sedimentary normal faults and the encased minibasins to the west (see Fig. 3A for location) and location of fault kinematic sites; (B) Un-interpreted and interpreted view towards the NW of the Emirhan weld characterized both by complete and incomplete weld with remnant gypsum that represents a cusp at the halokinetic sequence boundary, defined as tapered CHS in the lower Karayün strata of the Ilkindi margin minibasin to the south which are affected by strike slip faults with dextral motion connected to the salt weld (see Fig. 5A for location). (C) Interpreted satellite image of the upper part of the Lower Member of the Karayün Fm showing a succession of Hook halokinetic sequences with unconformities and axial traces forming a tabular composite halokinetic sequences (CHS) along evaporite weld separating the Emirhan minibasin to the east and the Köy minibasin (see Fig. 5A for location; Image courtesy of Google Earth).

Fig. 6. Detailed geological map of the tilted Arpayazi, Karayün and Eğribuçak minibasins showing tapered CHS, wedge HS, halokinetic fold, trace of unconformities, megaflap, welds, strike-slip faults and syn-sedimentary normal faults and location of fault kinematic measurements sites (see Fig. 3A for location).

Fig. 7. (A) Geoeye satellite colour composite image of the east Karayün minibasin, where vertical to overturned strata make the map view pattern roughly equivalent to a cross-section. Lower and Middle Karayün members become progressively thinned and drape-folded along the edge of the diapir, forming a large megaflap whose limb is overturned close the Akpinar minibasin (Fig. 6 for location). (B) Geoeye satellite colour composite image of the limb of the Karayün megaflap and the western margin of the Akpınar minibasin. (C) Geological map of the folded limb of the Karayün megaflap and the western margin of the Akpınar minibasin showing Tapered CHS within the base of the Karacaören Fm (see Fig. 7A for location).

Fig. 8. (A) Geological map of the encapsulated Inceyol minibasin with location of the cross-section presented on Fig. 8C (see Fig. 5A for location). (B) Overview of an encapsulated minibasin, the Inceyol minibasin and associated salt diapir (see Fig. 8A for location). (C) Schematic cross-section passing through the encapsulated Inceyol minibasin showing two isolated tight synclines delimited by a thinned to squeezed salt diapir (see Fig. 5A for location).

Fig. 9. (A) View toward the east showing an erosive unconformity that separates the Selimiye Fm from the Karacaören Fm, with high-angle unconformities up to 90° between the marine Karacaören beds and the folded beds of the Selimiye Fm in the Celallı anticline (see Fig. 4, location b). (B) View toward the west showing the major marine unconformity characterized by high-angle discordance affecting the limb of the halokinetic drap-folding made of Karayün Fm and covering by onlap the Karacaören Fms with onlaps along eastern Emirhan minibasin margin (see Fig. 4 for location).

Fig. 10. (A) View toward the north-west showing showing the Tuzhisar Thrust (AT) hanging-wall formed by a large stratigraphic wedge with N-S trending beds thinning towards the south over a zone more than 2000m wide. (B) View toward the east showing the Ağılkaya Thrust (AT) hanging-wall formed by the Ağılkaya minibasin characterized by two synclines with an axis at right angle to the north-south regional shortening direction exposing dissymmetric halokinetic wedges on both flanks, with vertical to overturned strata thinning over a shorter distance on the northern flanks (see Fig. 4 for location).

Fig. 11. View toward the east of the Gölcük Thrust (GT) passing through salt walls associated with megaclasts of serpentinized peridotite, separating the Karayün and Akpınar minibasin to the NW from the Celallı anticline to the SE, showing growth syncline in footwall position making of Benlikaya Fm (see Fig. 4 for location).

Fig. 12. Stereo plot of strike-slip fault zone showing fault kinematics located along minibasin edges, see Fig. for location.

Fig. 13. (A) Geological map of the Çaygören and northern part of the Eğribuçak minibasins separated by the Çaygören wall, with locations around the salt sheet section within the Çaygören (see Fig. 3A for location). (B) Un-interpreted and interpreted view towards the NW of the Çaygören minibasin showing large wedge halokinetic sequence and interpreted section of the salt sheet showing recumbent folds extending over tens of meters with a north vergence (see Fig. 13A for location). (C) View of flat contact beneath the salt sheet showing concordant strata with the only evidence of normal faults within the Benlikaya strata and no evidence of shear faults (see Fig. 13 B for location). (D) View of ramp contact beneath the salt sheet characterized by a shear zone, up to 1 m wide, delimiting sandstone lenses and boudins displaying clockwise rotation, related to a dextral motion (see Fig. 13B for location).

Fig. 14. N-S cross-sections across the secondary minibasins (WAB domain) of the Sivas Basin based on the seismic interpretation from surface data and Fig. 3B (see location on Fig. 3A). The sections illustrate mainly the geometry of secondary minibasins, which are well constrained at the surface but poorly constrained at depth due to the presence of both allochthonous and autochthonous salt levels. Thus, several geometries, thicknesses and basement configurations are possible. Bedding attitudes are indicated by short black dashed lines and welds by pairs of dots.

Fig. 15. Tectono-stratigraphic diagrams of the Karayün, Karacaören and Benlikaya formations in the studied mini-basins. (A) Depositional model illustrating minibasin structures and sedimentary pattern of the Lower member of the Karayün formation. Minibasin margins are formed by local composite halokinetic sequences developed along both East-West and North-South directions resulting in the formation of a polygonal network of salt anticlines with pillows at their intersection surrounding isolated, subcircular to elliptical basins. Structures and sediment distribution across this area are influenced by the salt-induced local accommodation, generated by salt withdrawal (e.g. Ribes et al., 2015; Ribes et al., 2016). (B) Depositional model illustrating minibasin structures and sedimentary pattern of the Middle member of the Karayün Formation, showing a globally isopachous sedimentary package covering both preexisting depocenter and salt structures. Small thickness variations reflect the crests of salt structures showing the weak influence of halokinesis. At the top of preexisting salt structures, syn-sedimentary normal faults cut this coarser sedimentary package, recording the local influence of salt withdrawal, which is weak but still active. The relative abrupt increase of sedimentary rate in the minibasin province is attributed to a regional uplift of the southern margin of the basin (Kergaravat et al., 2016). (C) Depositional model illustrating minibasin structures and sedimentary pattern of the Upper member of the Karayün Formation, showing large halokinetic folding and even megaflaps development associated with rejuvenation of diapirs and formation of encapsulated minibasins. Structures and sediment distribution across this area are influenced by the rejuvenation of salt diapir leading to minibasin disconnection and important salt topography feeding encapsulated minibasins. (D) Depositional model illustrating minibasin structures and sedimentary pattern of the Karacaören Formation, showing linear depocenter with preferentially large stratigraphic wedges along salt walls. Structures and sediment distribution across this area are influenced by the squeeze of preexisting evaporite walls at right angle to the regional shortening direction. (E) Depositional model illustrating minibasin structures and sedimentary pattern of the Benlikaya Formation, showing the squeezing of salt structure leading to the formation of thrust faults passing through preexisting salt walls, allochthonous salt and salt weld, which are developed both at right angles and oblique to the regional shortening direction. Structures and sediment distribution across this area are influenced by the regional shortening associated with the squeeze of the salt structures and the tilting of minibasins in the central area.

Fig. 16. Conceptual models of minibasin province illustrating stratal geometries and salt structures pattern showing the influence of shortening and salt thickness during sinking of minibasin, diagrams a and b, and on pre-existing minibasins province with polygonal and linear salt structures, diagrams c, based on interpretation of the Sivas minibasins.

Fig. 17. Synoptic models illustrating the possible origin of the Sivas minibasin tilting: (a) The advance of the fold and thrust belt underneath the minibasins is accommodated by the formation of thrust sheets; (b) The subsalt tilting may induce the gliding of the minibasins toward the center of minibasin area; (c) The heterogeneity of the domain located below the salt canopy, including primary minibasins and early salt feeders results in a pre-canopy basal topography.

11.REFERENCES

Artan, U., Sestini, G., 1971. Geology of the Beypinari-Karababa area (Sivas province). Bulletin Mineral Research and Exploration (Ankara, Turkey) 76, 72-89.

Brun, J.-P., Fort, X., 2004. Compressional salt tectonics (Angolan margin). Tectonophysics 382, 129-150.

954 Callot, J.-P., Ribes, C., Kergaravat, C., Bonnel, C., Temiz, H., Poisson, A., Vrielynck, B., Salel, J.-F.,
955 Ringenbach, J.-C., 2014. Salt tectonics in the Sivas basin (Turkey): crossing salt walls and
956 minibasins. Bulletin de la Societe Geologique de France 185, 33-42.
957 Callot, J.-P., Salel, J.-F., Letouzey, J., Daniel, J.-M., Ringenbach, J.-C., 2016. Three-dimensional
958 evolution of salt-controlled minibasins: Interactions, folding, and megaflap development.
959 AAPG Bulletin 100, 1419-1442.
960 Callot, J.P., Jahani, S., Letouzey, J., 2007. The role of pre-existing diapirs in fold and thrust belt
961 development. Thrust belts and foreland basins, 309-325.
962 Callot, J.P., Trocme, V., Letouzey, J., Albouy, E., Jahani, S., Sherkati, S., 2012. Pre-existing salt
963 structures and the folding of the Zagros Mountains. in Alsop, G.I., Archer, S.G., Hartley, A.J.,
964 Grant, N.T. & Hodgkinson, R. (eds) Salt Tectonics, Sediments and Prospectivity. Geological
965 Society, London, Special Publications 363, 545-561.
966 Cartwright, J., Jackson, M., Dooley, T., Higgins, S., 2012. Strain partitioning in gravity-driven
967 shortening of a thick, multilayered evaporite sequence. Geological Society, London, Special
968 Publications 363, 449-470.
969 Cater, J.M.L., Hanna, S.S., Ries, A.C., Turner, P., 1991. Tertiary evolution of the Sivas Basin, central
970 Turkey. Tectonophysics 195, 29-46.
971 Çiner, A., Kosun, E., Deynoux, M., 2002. Fluvial, evaporitic and shallow-marine facies architecture,
972 depositional evolution and cyclicity in the Sivas Basin (Lower to Middle Miocene), Central
973 Turkey. Journal of Asian Earth Sciences 21, 147-165.
974 Collon, P., Pichat, A., Kergaravat, C., Botella, A., Caumon, G., Ringenbach, J.-C., Callot, J.-P., 2016. 3D
975 modeling from outcrop data in a salt tectonic context: Example from the Inceyol minibasin,
976 Sivas Basin, Turkey. Interpretation 4, SM17-SM31.
977 Diegel, F.A., Karlo, J., Schuster, D., Shoup, R., Tauvers, P., 1995. Cenozoic structural evolution and
978 tectono-stratigraphic framework of the northern Gulf Coast continental margin. in M. P. A.
979 Jackson, D. G. Roberts, and S. Snelson, eds., Salt tectonics, a global perspective: AAPG Memoir
980 65, 109-151.
981 Dooley, T.P., Hudec, M.R., Jackson, M.P.A., 2012. The structure and evolution of sutures in
982 allochthonous salt. AAPG Bulletin 96, 1045-1070.
983 Dooley, T.P., Jackson, M.P., Hudec, M.R., 2009. Inflation and deflation of deeply buried salt stocks
984 during lateral shortening. Journal of Structural Geology 31, 582-600.
985 Dooley, T.P., Jackson, M.P., Hudec, M.R., 2013. Coeval extension and shortening above and below
986 salt canopies on an uplifted, continental margin: Application to the northern Gulf of Mexico.
987 AAPG Bulletin 97, 1737-1764.
988 Duffy, O.B., Fernandez, N., Hudec, M.R., Jackson, M.P., Burg, G., Dooley, T.P., Jackson, C.A.-L., 2017.
989 Lateral mobility of minibasins during shortening: Insights from the SE Precaspian Basin,
990 Kazakhstan. Journal of Structural Geology 97, 257-276
991 Erik, N.Y., Aydemir, A., Buyuksarac, A., 2015. Investigation of the organic matter properties and
992 hydrocarbon potential of the Sivas Basin, Central Eastern Anatolia, Turkey, using Rock-Eval
993 data and organic petrography. Journal of Petroleum Science and Engineering 127, 148-168.
994 Fort, X., Brun, J.P., Chauvel, F., 2004. Contraction induced by block rotation above salt (Angolan
995 margin). Marine and Petroleum Geology 21, 1281-1294.
996 Giles, K.A., Lawton, T.F., 2002. Halokinetic sequence stratigraphy adjacent to the El Papalote diapir,
997 northeastern Mexico. AAPG bulletin 86, 823-840.
998 Giles, K.A., Rowan, M.G., 2012. Concepts in halokinetic-sequence deformation and stratigraphy. in
999 Alsop, G.I., Archer, S.G., Hartley, A.J., Grant, N.T. & Hodgkinson, R. (eds) Salt Tectonics,
1000 Sediments and Prospectivity. Geological Society, London, Special Publications 363, 7-31.
1001 Görür, N., Tüysüz, O., Celal Şengör, A., 1998. Tectonic evolution of the central Anatolian basins.
1002 International Geology Review 40, 831-850.
1003 Graham, R., Jackson, M., Pilcher, R., Kilsdonk, B., 2012. Allochthonous salt in the sub-Alpine fold-
1004 thrust belt of Haute Provence, France. in Alsop, G.I., Archer, S.G., Hartley, A.J., Grant, N.T. &

Hodgkinson, R. (eds) Salt Tectonics, Sediments and Prospectivity. Geological Society, London, Special Publications 363, 595-615.

Guezou, J.C., Temiz, H., Poisson, A., Gürsoy, H., 1996. Tectonics of the Sivas Basin: The Neogene Record of the Anatolian Accretion Along the Inner Tauric Suture. International Geology Review 38, 901-925.

Gündogan, I., Önal, M., Depçi, T., 2005. Sedimentology, petrography and diagenesis of Eocene–Oligocene evaporites: the Tuzhisar Formation, SW Sivas Basin, Turkey. Journal of Asian Earth Sciences 25, 791-803.

Harrison, J.C., Jackson, M.P.A., 2014. Exposed evaporite diapirs and minibasins above a canopy in central Sverdrup Basin, Axel Heiberg Island, Arctic Canada. Basin Research 26, 567-596.

Hearon, T.E., Rowan, M.G., Lawton, T.F., Hannah, P.T., Giles, K.A., 2015. Geology and tectonics of Neoproterozoic salt diapirs and salt sheets in the eastern Willouran Ranges, South Australia. Basin Research 27, 183-207.

Hudec, M.R., Jackson, M.P., Schultz-Ela, D.D., 2009. The paradox of minibasin subsidence into salt: Clues to the evolution of crustal basins. Geological Society of America Bulletin 121, 201-221.

Hudec, M.R., Jackson, M.P.A., 2007. Terra infirma: Understanding salt tectonics. Earth-Science Reviews 82, 1-28.

Huvaz, O., 2009. Comparative petroleum systems analysis of the interior basins of Turkey: implications for petroleum potential. Marine and Petroleum Geology 26, 1656-1676.

Jackson, C.a.L., Jackson, M.P.a., Hudec, M.R., Rodriguez, C., 2014. Internal structure, kinematics, and growth of a salt wall: Insights from 3-D seismic data. Geology 42, 307-310.

Jackson, C.A.L., Kane, K.E., Larsen, E., 2010. Structural evolution of minibasins on the Utsira High, northern North Sea; implications for Jurassic sediment dispersal and reservoir distribution. Petroleum Geoscience 16, 105-120.

Jackson, M.P., Cornelius, R., Craig, C., Gansser, A., Stöcklin, J., Talbot, C., 1990. Salt diapirs of the Great Kavir, central Iran. Geological Society of America Memoirs 177, 1-150.

Jackson, M.P.A., Harrison, J.C., 2006. An allochthonous salt canopy on Axel Heiberg Island, Sverdrup Basin, Arctic Canada. Geology 34, 1045-1048.

Jahani, S., Callot, J.P., Letouzey, J., Frizon de Lamotte, D., 2009. The eastern termination of the Zagros Fold-and-Thrust Belt, Iran: Structures, evolution, and relationships between salt plugs, folding, and faulting. Tectonics 28.

Karaoğlan, F., Parlak, O., Kloetzli, U., Thoeni, M., Koller, F., 2013. U–Pb and Sm–Nd geochronology of the Kızıldağ (Hatay, Turkey) ophiolite: implications for the timing and duration of suprasubduction zone type oceanic crust formation in the southern Neotethys. Geological Magazine 150, 283-299.

Kergaravat, C., 2016. Dynamique de formation et de déformation de mini-bassins en contexte compressif : exemple du bassin de Sivas (Turquie), approche terrain et implications structurales multi-échelles. PhD Thesis. Université de Pau et des Pays de l'Adour.

Kergaravat, C., Ribes, C., Legeay, E., Callot, J.P., Kavak, K.S., Ringenbach, J.C., 2016. Minibasins and salt canopy in foreland fold-and-thrust belts: The central Sivas Basin, Turkey. Tectonics 35, DOI 10.1002/2016TC004186

Kernen, R.A., Giles, K.A., Rowan, M.G., Lawton, T.F., Hearon, T.E., 2012. Depositional and halokinetic-sequence stratigraphy of the Neoproterozoic Wonoka Formation adjacent to Patawarta allochthonous salt sheet, Central Flinders Ranges, South Australia. in Alsop, G.I., Archer, S.G., Hartley, A.J., Grant, N.T. & Hodgkinson, R. (eds) Salt Tectonics, Sediments and Prospectivity. Geological Society, London, Special Publications 363, 81-105.

Kluth, C.F., DuChene, H.R., 2009. Late Pennsylvanian and Early Permian structural geology and tectonic history of the Paradox Basin and Uncompahgre Uplift, Colorado and Utah. in Houston et al., The Paradox Basin Revisited – New Developments in Petroleum Systems and Basin Analysis: RMAG Special Publication, 178-197.

Kurtman, F., 1973. Geologic and tectonic structure of the Sivas-Hafik-Zara and Imranli region. Bulletin Mineral Research and Exploration (Ankara, Turkey) 80, 1-32.

Lawton, T.F., Buck, B.J., 2006. Implications of diapir-derived detritus and gypsic paleosols in Lower Triassic strata near the Castle Valley salt wall, Paradox Basin, Utah. Geology 34, 885-885.

Letouzey, J., Colletta, B., Vially, R., Chermette, J., 1995. Evolution of salt-related structures in compressional settings. in, M. P. A. Jackson, D. G. Roberts, and S. Snelson, eds., Salt tectonics, a global perspective: AAPG Memoir 65, p 41-60.

López-Mir, B., Muñoz, J.A., García-Senz, J., 2015. Extensional salt tectonics in the partially inverted Cotiella post-rift basin (south-central Pyrenees): structure and evolution. International Journal of Earth Sciences 104, 419-434.

Martín-Martín, J.D., Vergés, J., Saura, E., Moragas, M., Messager, G., Baqués, V., Razin, P., Grélaud, C., Malaval, M., Joussiaume, R., 2017. Diapiric growth within an Early Jurassic rift basin: The Tazoult salt wall (central High Atlas, Morocco). Tectonics 36, 2-32.

Okay, A., Tüysüz, O., Satır, M., Özkan-Altiner, S., Altiner, D., Sherlock, S., Eren, R., 2006. Cretaceous and Triassic subduction-accretion, high-pressure–low-temperature metamorphism, and continental growth in the Central Pontides, Turkey. Geological Society of America Bulletin 118, 1247-1269.

Onal, K.M., Buyuksarac, A., Aydemir, A., Ates, A., 2008. Investigation of the deep structure of the Sivas Basin (innereast Anatolia, Turkey) with geophysical methods. Tectonophysics 460, 186-197.

Özcan, E., Less, G., Baydogan, E., 2009. Regional implications of biometric analysis of Lower Miocene larger foraminifera from Central Turkey. Micropaleontology, 559-588.

Özçelik, O., Altunsoy, M., 1996. Clastic petrofacies, provenance and organic facies of the Bozbel Formation (Lutetian) in the Eastern Sivas Basin (Turkey). Marine and Petroleum Geology 13, 493-501.

Paz, J.D.S., Rossetti, D.F., 2006. Petrography of gypsum-bearing facies of the Codó Formation (Late Aptian), Northern Brazil. Anais da Academia Brasileira de Ciências 78, 557-572.

Peel, F., Travis, C., Hossack, J., 1995. Genetic structural provinces and salt tectonics of the Cenozoic offshore US Gulf of Mexico: A preliminary analysis, in Salt Tectonics: A Global Perspective, AAPG Mem., vol. 65, edited by M. P. A. Jackson, D. G. Roberts, and S. Snelson, pp. 153–175, Tulsa, Okla.

Pichat, A., Hoareau, G., Callot, J.-P., Legeay, E., Kavak, K.S., Revillon, S., Parat, C., Ringenbach, J.-C., Submitted. Evidence of multiple evaporite recycling processes in a salt-tectonic context, Sivas Basin, Turkey. Terra Nova.

Pichat, A., Hoareau, G., Callot, J.-P., Ringenbach, J.-C., 2016. Diagenesis of Oligocene continental sandstones in salt-walled mini-basins—Sivas Basin, Turkey. Sedimentary Geology 339, 13-31.

Pilcher, R.S., Kilsdonk, B., Trude, J., 2011. Primary basins and their boundaries in the deep-water northern Gulf of Mexico: Origin, trap types, and petroleum system implications. AAPG Bulletin 95, 219-240.

Poisson, A., Guezou, J., Ozturk, A., Inan, S., Temiz, H., Gürsöy, H., Kavak, K., Özden, S., 1996. Tectonic setting and evolution of the sivas basin, Central anatolia, Turkey. International Geology Review 38, 838-853.

Poisson, A., Orszag-Sperber, F., Temiz, H., Vrielynck, B., 2010. Stratigraphic and polyphased tectonic evolution of the Sivas basin (central anatolia, Turkey). Darius annual report, consultable à Univ. PM Curie, Paris, 1-48.

Poisson, A., Vrielynck, B., Wernli, R., Negri, A., Bassetti, M.-A., Büyükmeriç, Y., Özer, S., Guillou, H., Kavak, K.S., Temiz, H., 2015. Miocene transgression in the central and eastern parts of the Sivas Basin (Central Anatolia, Turkey) and the Cenozoic palaeogeographical evolution. International Journal of Earth Sciences, 1-30.

Ribes, C., 2015. Interaction entre la tectonique salifère et la sédimentation dans des mini-bassins : Exemple de l'Oligo-Miocène du bassin de Sivas, Turquie. PhD Thesis. Université de Pau et des Pays de l'Adour.

Ribes, C., Kergaravat, C., Bonnel, C., Crumeyrolle, P., Callot, J.-P., Poisson, A., Temiz, H., Ringenbach, J.-C., 2015. Fluvial sedimentation in a salt-controlled mini-basin: stratal patterns and facies assemblages, Sivas Basin, Turkey. Sedimentology 62, 1513-1545.

Ribes, C., Kergaravat, C., Crumeyrolle, P., Lopez, M., Bonnel, C., Poisson, A., Kavak, K.S., Callot, J.-P., Ringenbach, J.-C., 2016. Factors controlling stratal pattern and facies distribution of fluvio-lacustrine sedimentation in the Sivas mini-basins, Oligocene (Turkey). Basin Research, n/a-n/a.

Ribes, C., Lopez, M., Crumeyrolle, P., Kergaravat, C., Poisson, A., Callot, J.P., Ringenbach, J.C., Submitted. Facies partitioning and stratal pattern on salt tectonics controlled shallow-marine to continental mini-basins: Examples from the Oligo-Miocene Formations of the Sivas Basin, Turkey.

Ringenbach, J.-C., Salel, J.-F., Kergaravat, C., Ribes, C., Bonnel, C., Callot, J.-P., 2013. Salt tectonics in the Sivas Basin, Turkey: outstanding seismic analogues from outcrops. first break 31, 93-101.

Rolland, Y., Galoyan, G., Sosson, M., Melkonyan, R., Avagyan, A., 2010. The Armenian Ophiolite: insights for Jurassic back-arc formation, Lower Cretaceous hot spot magmatism and Upper Cretaceous obduction over the South Armenian Block. Geological Society, London, Special Publications 340, 353-382.

Rowan, M.G., Giles, K.A., Hearon IV, T.E., Fiduk, J.C., 2016. Megaflaps adjacent to salt diapirs. AAPG Bulletin 100, 1723-1747.

Rowan, M.G., Inman, K.F., 2011. Salt-related deformation recorded by allochthonous salt rather than growth strata. Gulf Coast Association of Geological Societies Transactions, v. 61, p. 379–390.

Rowan, M.G., Lawton, T.F., Giles, K.A., 2012. Anatomy of an exposed vertical salt weld and flanking strata, La Popa Basin, Mexico. Geological Society, London, Special Publications 363, 33-57.

Rowan, M.G., Lawton, T.F., Giles, K.A., Ratliff, R.A., 2003. Near-salt deformation in La Popa basin, Mexico, and the northern Gulf of Mexico: A general model for passive diapirism. AAPG bulletin 87, 733-756.

Rowan, M.G., Vendeville, B.C., 2006. Foldbelts with early salt withdrawal and diapirism: Physical model and examples from the northern Gulf of Mexico and the Flinders Ranges, Australia. Marine and Petroleum Geology 23, 871-891.

Saura, E., Ardèvol i Oró, L., Teixell, A., Vergés, J., 2015. Rising and falling diapirs, shifting depocenters and flap overturning in the Cretaceous Sopeira and Sant Gervàs subbasins (Ribagorça basin, Southern Pyrenees). Tectonics, 35, doi:10.1002/2015TC004001.

Saura, E., Verges, J., Martin-Martin, J.D., Messager, G., Moragas, M., Razin, P., Grelaud, C., Joussiaume, R., Malaval, M., Homke, S., Hunt, D.W., 2014. Syn- to post-rift diapirism and minibasins of the Central High Atlas (Morocco): the changing face of a mountain belt. Journal of the Geological Society 171, 97-105.

Sherkati, S., Letouzey, J., 2004. Variation of structural style and basin evolution in the central Zagros (Izeh zone and Dezful Embayment), Iran. Marine and Petroleum Geology 21, 535-554.

Sherkati, S., Letouzey, J., Frizon de Lamotte, D., 2006. Central Zagros fold-thrust belt (Iran): New insights from seismic data, field observation, and sandbox modeling. Tectonics 25.

Sirel, E., Özgen-Erdem, N., Kangal, Ö., 2013. Systematics and biostratigraphy of Oligocene (Rupelian-Early Chattian) foraminifera from lagoonal-very shallow water limestone in the eastern Sivas Basin (central Turkey). Geol. Croatia 66, 83-110.

Stampfli, G.M., 2000. Tethyan oceans. Geological Society, London, Special Publications 173, 1-23.

Temiz, H., 1996. Tectonostratigraphy and Thrust Tectonics of the Central and Eastern Parts of the Sivas Tertiary Basin, Turkey. International Geology Review 38, 957-971.

Temiz, H., Guezou, J.C., Poisson, A.M., 2000. Tectonostratigraphy and kinematics of the eastern end of the Sivas Basin (central eastern Turkey): implications for the so-called ' Anatolian block '. Geological Journal, 28(3-4), 239-250.

Vendeville, B., Nilsen, K., 1995. Episodic growth of salt diapirs driven by horizontal shortening, Salt, Sediment, and Hydrocarbons: Society of Economic Paleontologists and Mineralogists, Gulf Coast Section, 16th Annual Research Conference Program and Extended Abstracts, pp. 285-295.

1160 Wagner, B.H., Jackson, M.P., 2011. Viscous flow during salt welding. Tectonophysics 510, 309-326.
1161 Yılmaz, A., Yılmaz, H., 2006. Characteristic features and structural evolution of a post collisional basin:
1162 The Sivas Basin, Central Anatolia, Turkey. Journal of Asian Earth Sciences 27, 164-176.

Figure

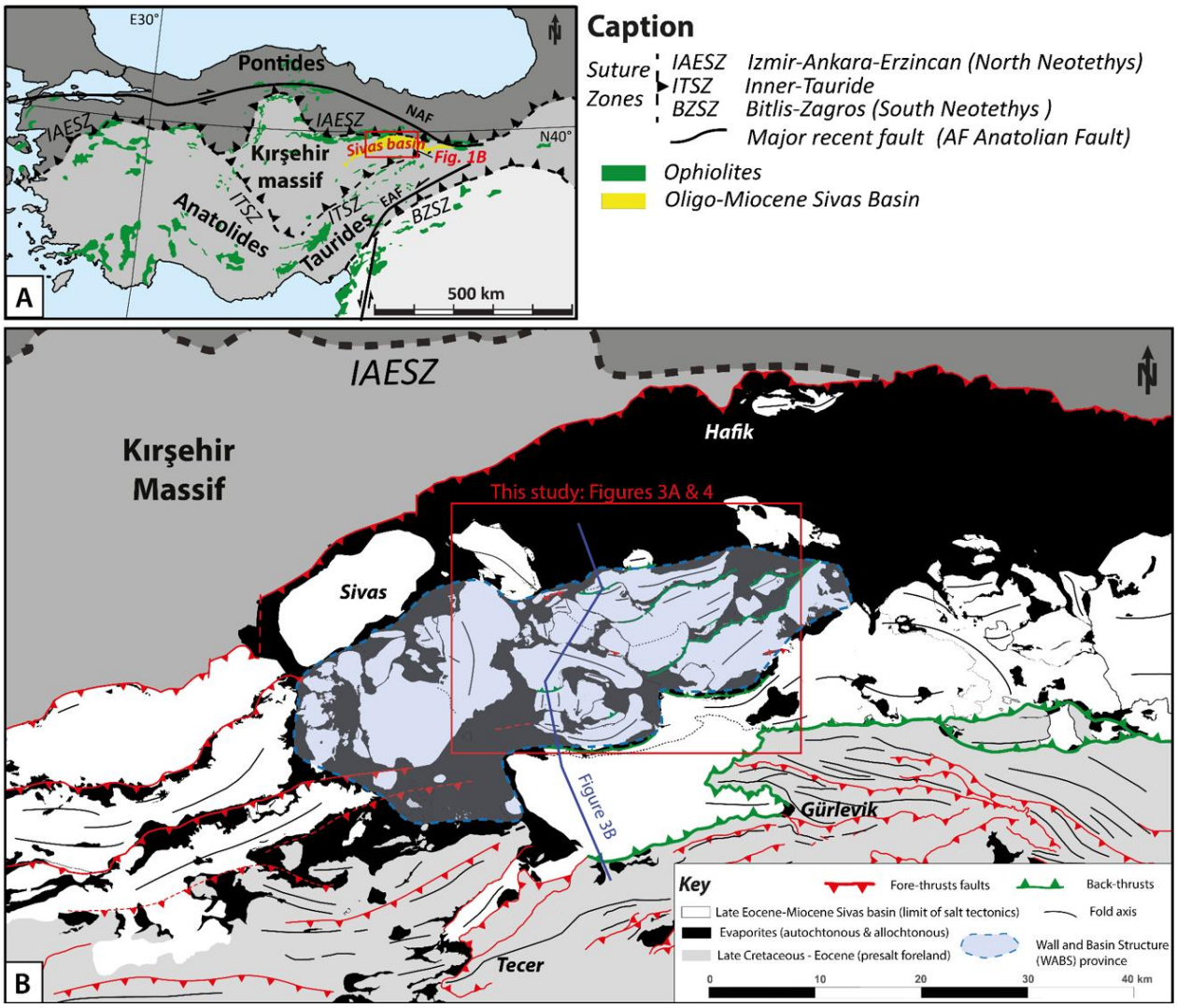
Caption
Suture Zones
IAESZ Izmir-Ankara-Erzincan (North Neotethys)
ITSZ Inner-Tauride
BZSZ Bitlis-Zagros (South Neotethys)
Major recent fault (AF Anatolian Fault)
Ophiolites
Oligo-Miocene Sivas Basin
E30°
N40°
Pontides
IAESZ
NAF
Kırşehir massif
Sivas basin
Fig. 1B
ITSZ
Anatolides
Taurides
EAF
BZSZ
500 km
A
IAESZ
Kırşehir Massif
Hafik
This study: Figures 3A & 4
Sivas
Figure 3B
Gürlevik
Tecer
B
Key
Fore-thrusts faults
Back-thrusts
Late Eocene-Miocene Sivas basin (limit of salt tectonics)
Fold axis
Evaporites (autochtonous & allochtonous)
Wall and Basin Structure (WABS) province
Late Cretaceous - Eocene (presalt foreland)
0
10
20
30
40 km

Fig. 1

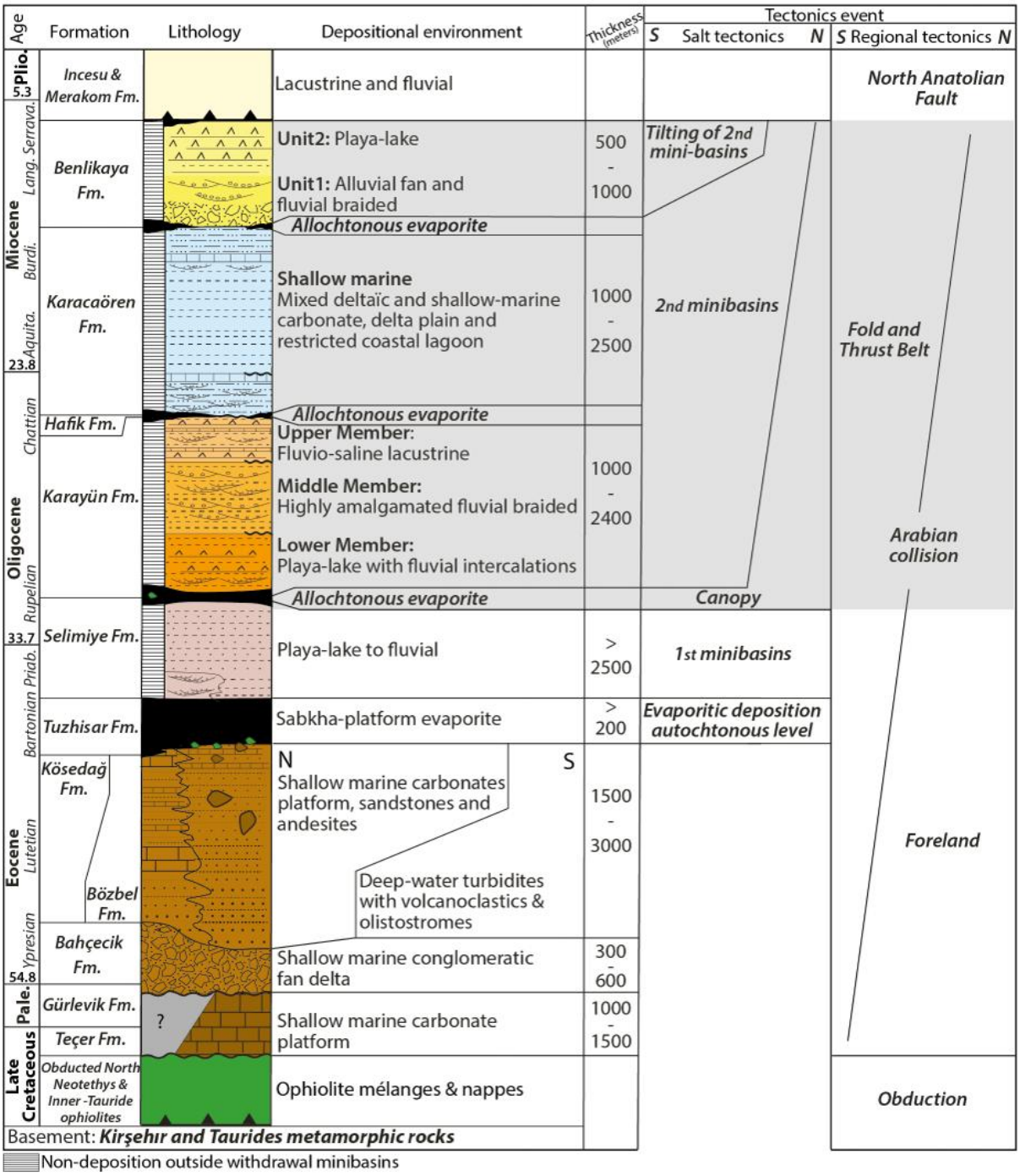
Age
Formation
Lithology
Depositional environment
Thickness (meters)
Tectonics event
S Salt tectonics N
S Regional tectonics N
Plio.
5.3
Incesu & Merakom Fm.
Lacustrine and fluvial
North Anatolian Fault
Miocene
Lang. Serrava.
Burdi.
Aquita.
23.8
Benlikaya Fm.
Unit2: Playa-lake
Unit1: Alluvial fan and fluvial braided
500 - 1000
Tilting of 2nd mini-basins
Allochtonous evaporite
Karacaören Fm.
Shallow marine
Mixed deltaïc and shallow-marine carbonate, delta plain and restricted coastal lagoon
1000 - 2500
2nd minibasins
Fold and Thrust Belt
Allochtonous evaporite
Oligocene
Chattian
Rupelian
33.7
Hafik Fm.
Karayün Fm.
Upper Member:
Fluvio-saline lacustrine
Middle Member:
Highly amalgamated fluvial braided
Lower Member:
Playa-lake with fluvial intercalations
1000 - 2400
Arabian collision
Allochtonous evaporite
Canopy
Selimiye Fm.
Playa-lake to fluvial
> 2500
1st minibasins
Bartonian
Priab.
Tuzhisar Fm.
Sabkha-platform evaporite
> 200
Evaporitic deposition autochtonous level
Eocene
Lutetian
Ypresian
54.8
Kösedağ Fm.
Bözbel Fm.
N
S
Shallow marine carbonates platform, sandstones and andesites
Deep-water turbidites with volcanoclastics & olistostromes
1500 - 3000
Foreland
Bahçecik Fm.
Shallow marine conglomeratic fan delta
300 - 600
Pale.
Gürlevik Fm.
?
Shallow marine carbonate platform
1000 - 1500
Late Cretaceous
Teçer Fm.
Obducted North Neotethys & Inner -Tauride ophiolites
Ophiolite mélanges & nappes
Obduction
Basement: Kirşehır and Taurides metamorphic rocks
Non-deposition outside withdrawal minibasins

Fig. 2

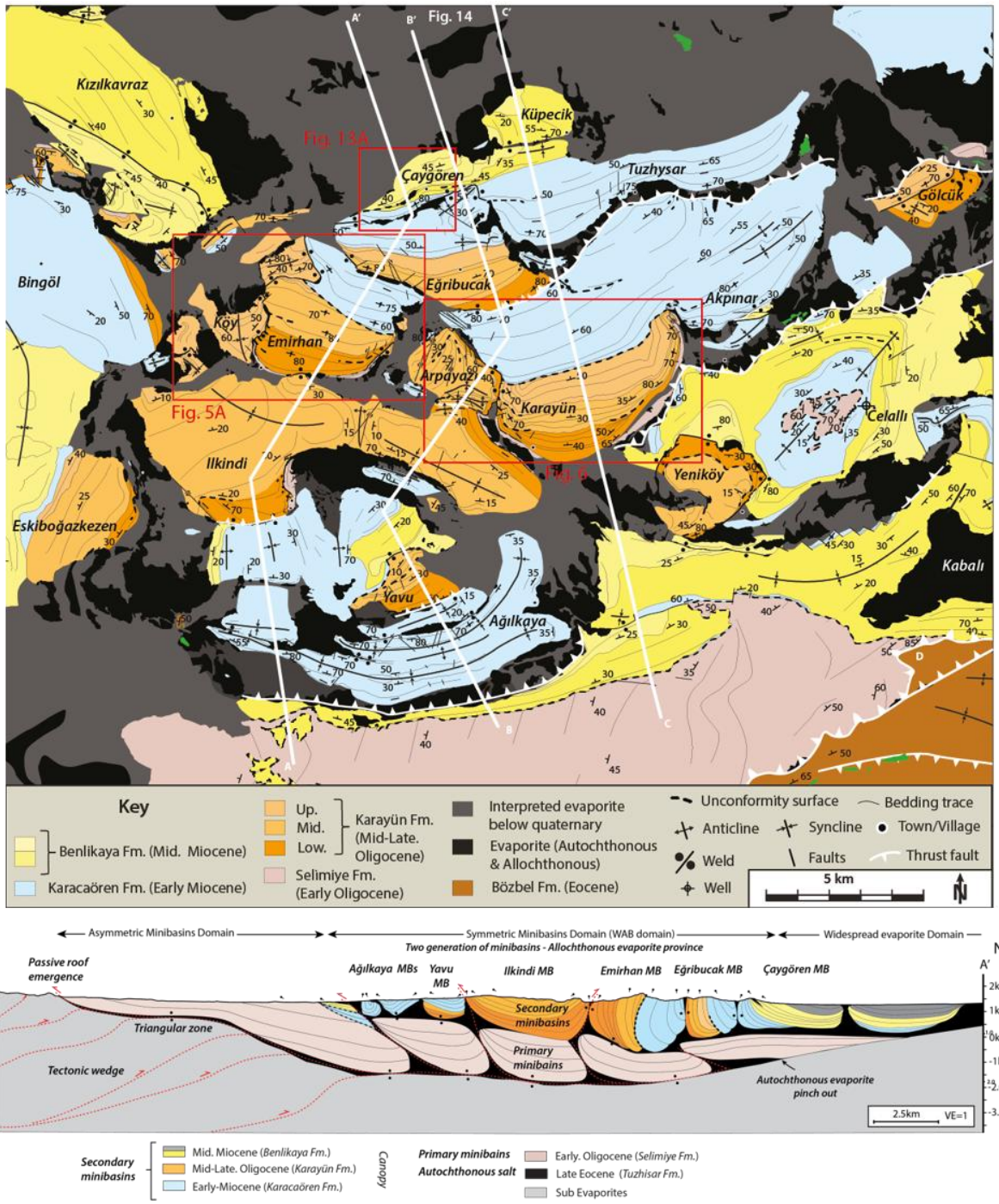
A'
B'
Fig. 14
C'
Kızılkavraz
Küpecik
Fig. 13A
Çaygören
Tuzhysar
Gölcük
Bingöl
Eğribucak
Akpınar
Köy
Emirhan
Arpayazı
Fig. 5A
Karayün
Celallı
Ilkindi
Fig. 6
Yeniköy
Eskiboğazkezen
Kabalı
Yavu
Ağılkaya
Key
Benlikaya Fm. (Mid. Miocene)
Karacaören Fm. (Early Miocene)
Up.
Mid.
Low.
Karayün Fm. (Mid-Late. Oligocene)
Selimiye Fm. (Early Oligocene)
Interpreted evaporite below quaternary
Evaporite (Autochthonous & Allochthonous)
Bözbel Fm. (Eocene)
Unconformity surface
Bedding trace
Anticline
Syncline
Town/Village
Weld
Faults
Thrust fault
Well
5 km
N

Asymmetric Minibasins Domain
Symmetric Minibasins Domain (WAB domain)
Widespread evaporite Domain
Two generation of minibasins - Allochthonous evaporite province
S
N
A
A'
Passive roof emergence
Ağılkaya MBs
Yavu MB
Ilkindi MB
Emirhan MB
Eğribucak MB
Çaygören MB
2km
1km
0km
-1km
-2.0km
-3.0km
Triangular zone
Tectonic wedge
Secondary minibasins
Primary minibains
Autochthonous evaporite pinch out
2.5km
VE=1
Secondary minibasins
Mid. Miocene (Benlikaya Fm.)
Mid-Late. Oligocene (Karayün Fm.)
Early-Miocene (Karacaören Fm.)
Canopy
Primary minibains
Autochthonous salt
Early. Oligocene (Selimiye Fm.)
Late Eocene (Tuzhisar Fm.)
Sub Evaporites

Fig. 3

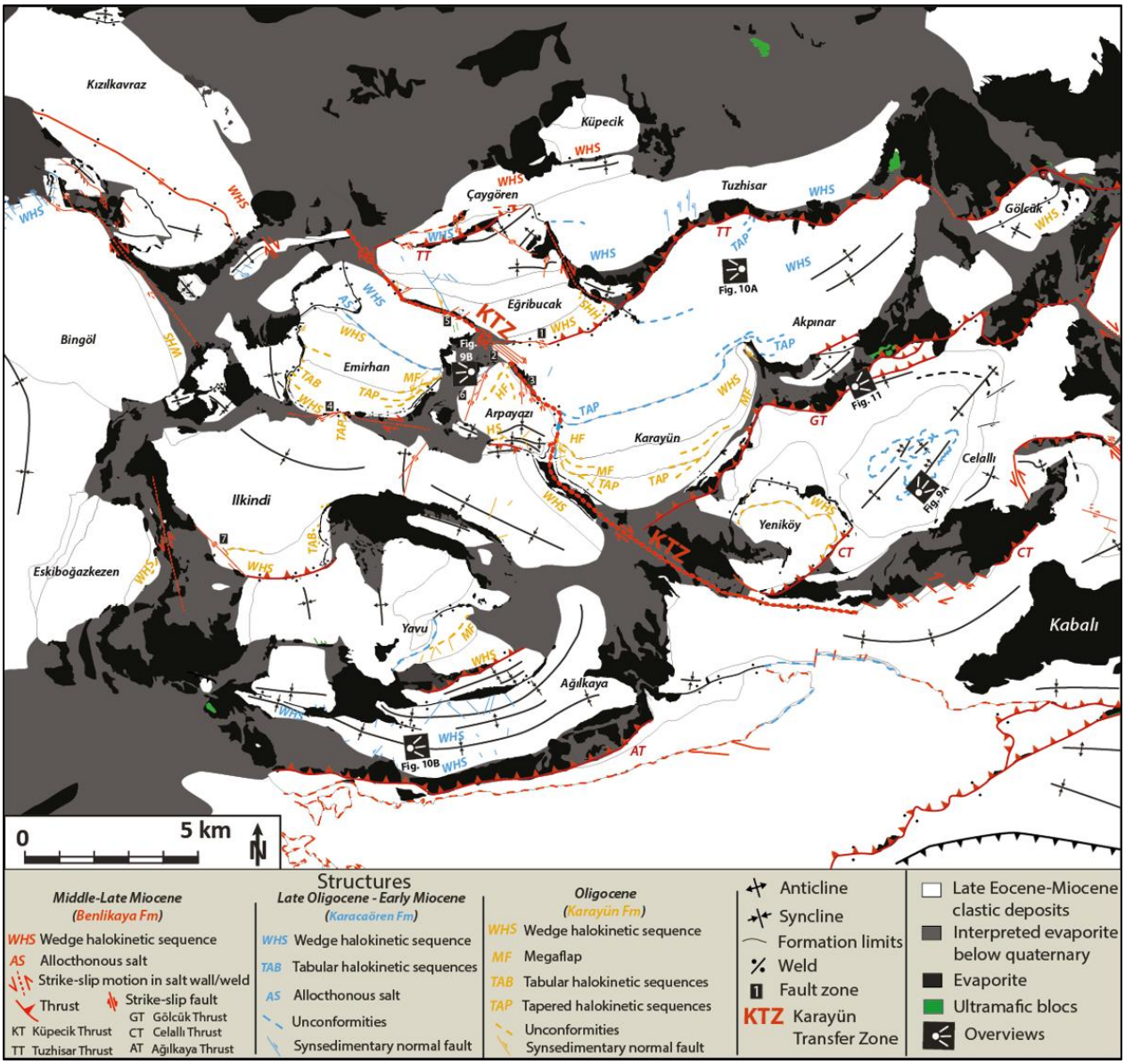
Kızılkavraz
Küpecik
Çaygören
Tuzhisar
Gölcük
Bingöl
Eğribucak
Akpınar
Emirhan
Arpayazı
Karayün
Celallı
Ilkindi
Yeniköy
Eskiboğazkezen
Yavu
Ağılkaya
Kabalı
Fig. 10A
Fig. 11
Fig. 9A
Fig. 9B
Fig. 10B
KTZ
WHS
TT
TAP
SHM
TAB
MF
HF
GT
CT
AT
0
5 km
N
Structures
Middle-Late Miocene (Benlikaya Fm)
WHS Wedge halokinetic sequence
AS Allocthonous salt
Strike-slip motion in salt wall/weld
Thrust
Strike-slip fault
KT Küpecik Thrust
GT Gölcük Thrust
TT Tuzhisar Thrust
CT Celallı Thrust
AT Ağılkaya Thrust
Late Oligocene - Early Miocene (Karacaören Fm)
WHS Wedge halokinetic sequence
TAB Tabular halokinetic sequences
AS Allocthonous salt
Unconformities
Synsedimentary normal fault
Oligocene (Karayün Fm)
WHS Wedge halokinetic sequence
MF Megaflap
TAB Tabular halokinetic sequences
TAP Tapered halokinetic sequences
Unconformities
Synsedimentary normal fault
Anticline
Syncline
Formation limits
Weld
Fault zone
KTZ Karayün Transfer Zone
Late Eocene-Miocene clastic deposits
Interpreted evaporite below quaternary
Evaporite
Ultramafic blocs
Overviews

Fig. 4

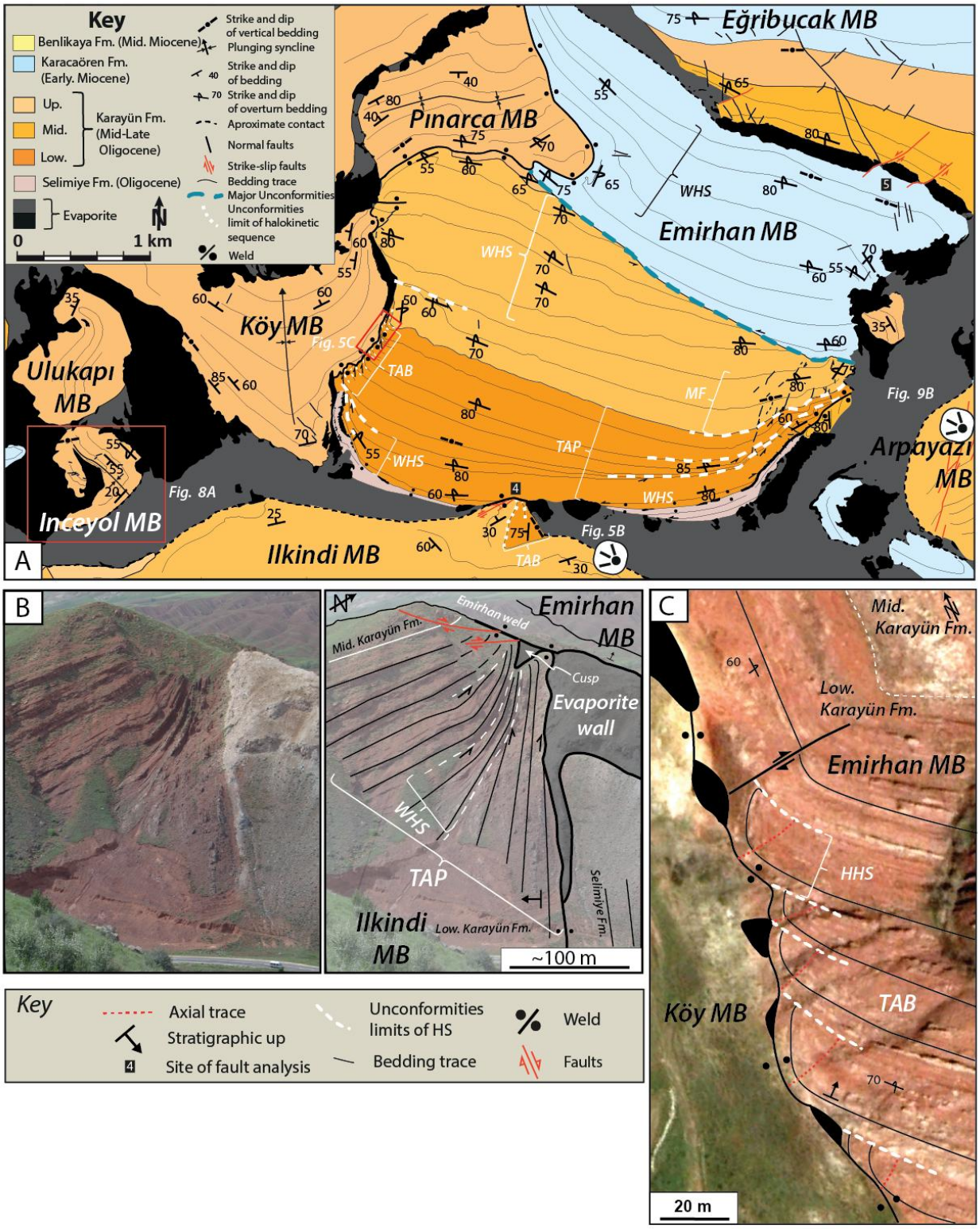
Key
Benlikaya Fm. (Mid. Miocene)
Karacaören Fm. (Early. Miocene)
Up.
Mid.
Low.
Karayün Fm. (Mid-Late Oligocene)
Selimiye Fm. (Oligocene)
Evaporite
0
1 km
Strike and dip of vertical bedding
Plunging syncline
Strike and dip of bedding
Strike and dip of overturn bedding
Aproximate contact
Normal faults
Strike-slip faults
Bedding trace
Major Unconformities
Unconformities limit of halokinetic sequence
Weld
Eğribucak MB
Pınarca MB
Emirhan MB
Köy MB
Ulukapı MB
İnceyol MB
Ilkindi MB
Arpayazı MB
WHS
TAB
TAP
MF
HHS
Fig. 5C
Fig. 8A
Fig. 5B
Fig. 9B
A
B
C
Emirhan weld
Mid. Karayün Fm.
Low. Karayün Fm.
Cusp
Evaporite wall
Selimiye Fm.
~100 m
20 m
Key
Axial trace
Stratigraphic up
Site of fault analysis
Unconformities limits of HS
Bedding trace
Weld
Faults

Fig. 5

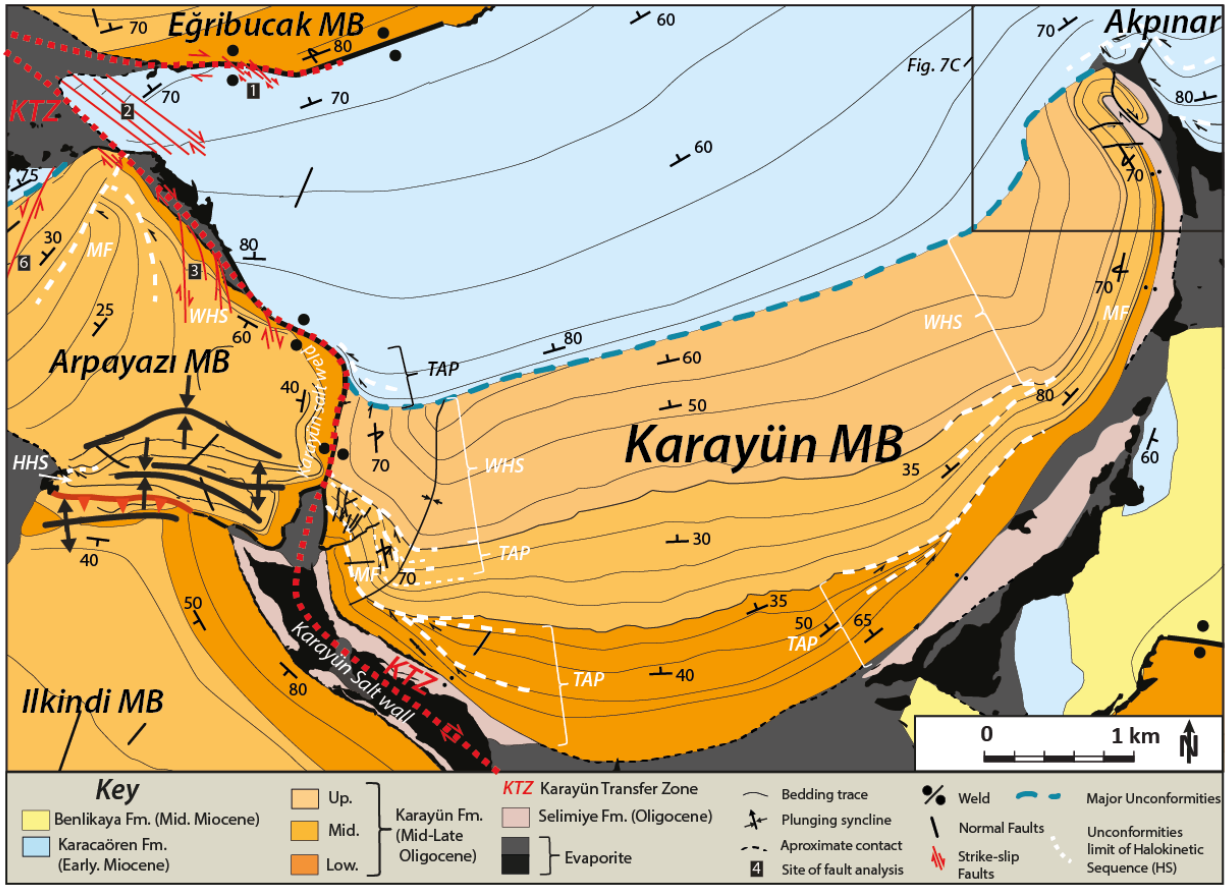
Eğribucak MB
Akpınar
Fig. 7C
KTZ
MF
WHS
TAP
HHS
Arpayazı MB
Karayün MB
Ilkindi MB
Karayün Salt wall
0
1 km
Key
Benlikaya Fm. (Mid. Miocene)
Karacaören Fm. (Early. Miocene)
Up.
Mid.
Low.
Karayün Fm. (Mid-Late Oligocene)
KTZ Karayün Transfer Zone
Selimiye Fm. (Oligocene)
Evaporite
Bedding trace
Plunging syncline
Aproximate contact
Site of fault analysis
Weld
Normal Faults
Strike-slip Faults
Major Unconformities
Unconformities limit of Halokinetic Sequence (HS)

Fig. 6

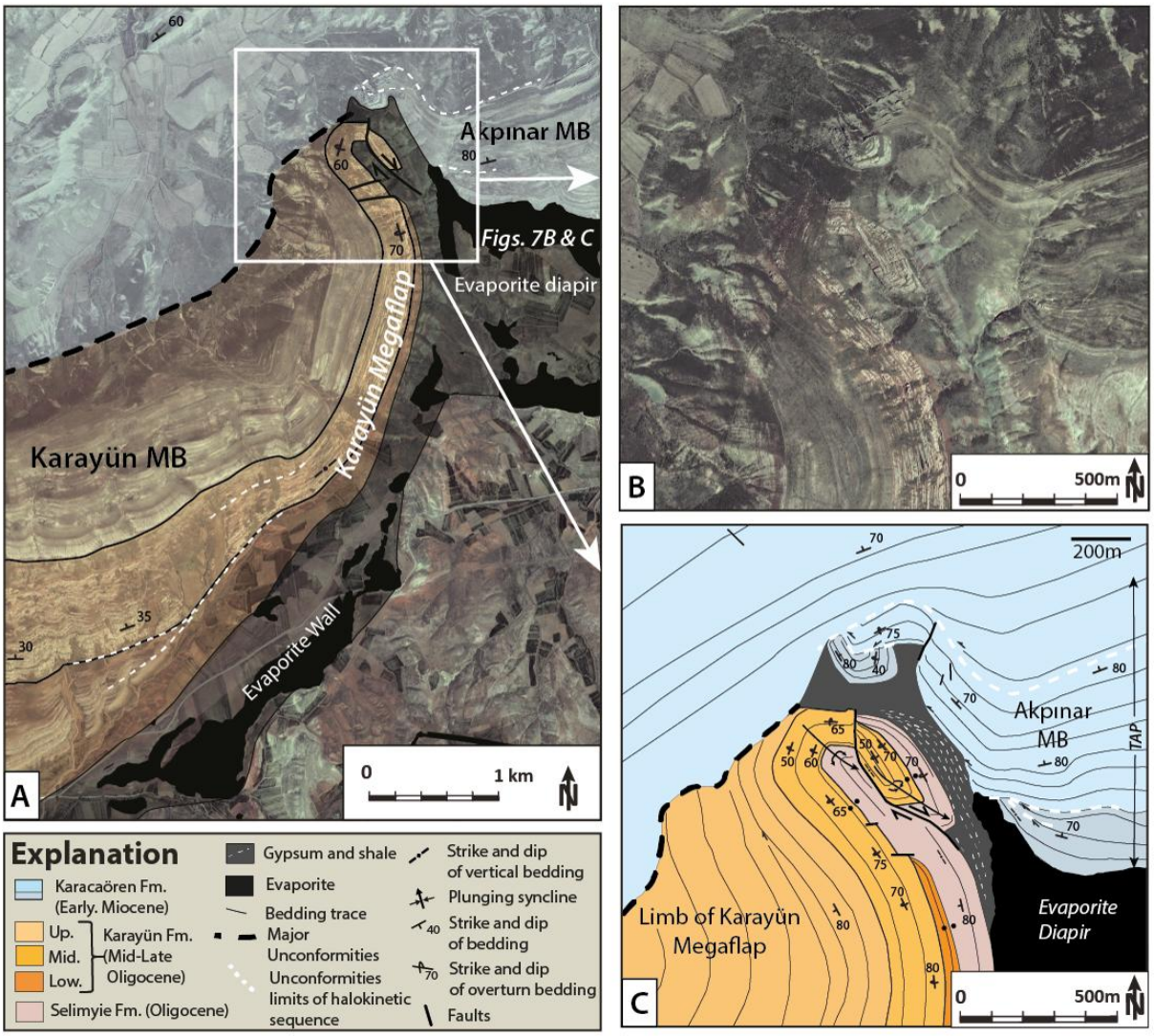
Akpınar MB
Figs. 7B & C
Evaporite diapir
Karayün Megaflap
Karayün MB
Evaporite Wall
A
0
1 km
B
0
500m
200m
Akpınar MB
TAP
Limb of Karayün Megaflap
Evaporite Diapir
C
0
500m
Explanation
Karacaören Fm. (Early. Miocene)
Up.
Mid.
Low.
Karayün Fm. (Mid-Late Oligocene)
Selimyie Fm. (Oligocene)
Gypsum and shale
Evaporite
Bedding trace
Major Unconformities
Unconformities limits of halokinetic sequence
Strike and dip of vertical bedding
Plunging syncline
Strike and dip of bedding
Strike and dip of overturn bedding
Faults

Fig. 7

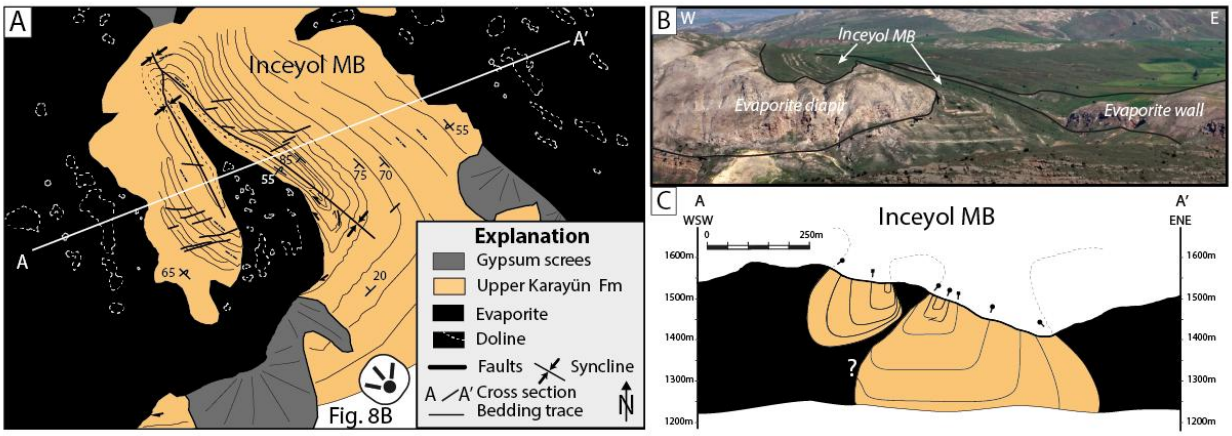
A
Inceyol MB
A'
A
55
55
75
70
65
20
Fig. 8B
Explanation
Gypsum screes
Upper Karayün Fm
Evaporite
Doline
Faults
Syncline
A A' Cross section
Bedding trace
N
B
W
E
Inceyol MB
Evaporite diapir
Evaporite wall
C
A
WSW
A'
ENE
Inceyol MB
0
250m
1600m
1500m
1400m
1300m
1200m
?

Fig. 8

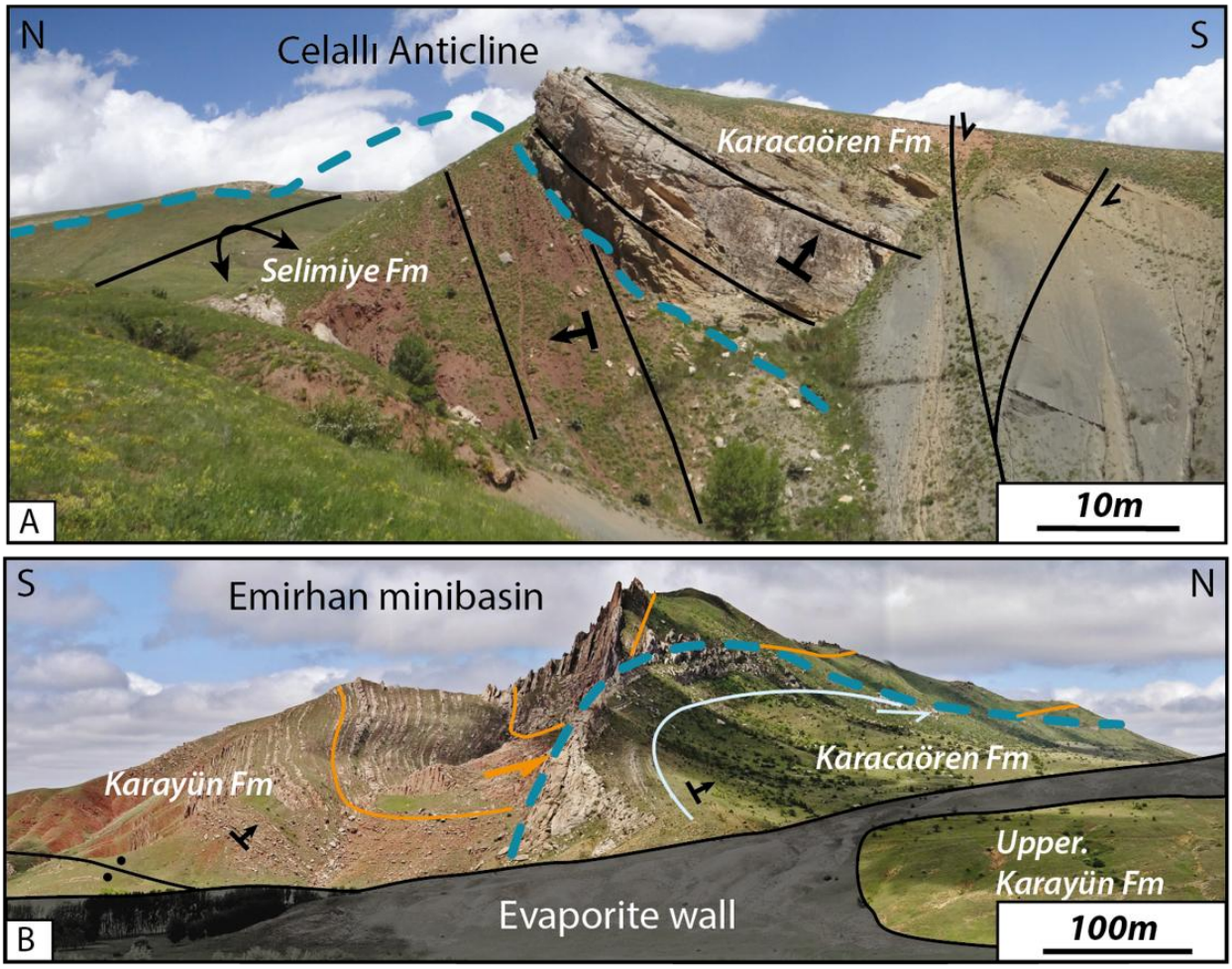
N
Celallı Anticline
S
Karacaören Fm
Selimiye Fm
10m
A
S
Emirhan minibasin
N
Karayün Fm
Karacaören Fm
Upper.
Karayün Fm
Evaporite wall
100m
B

Fig. 9

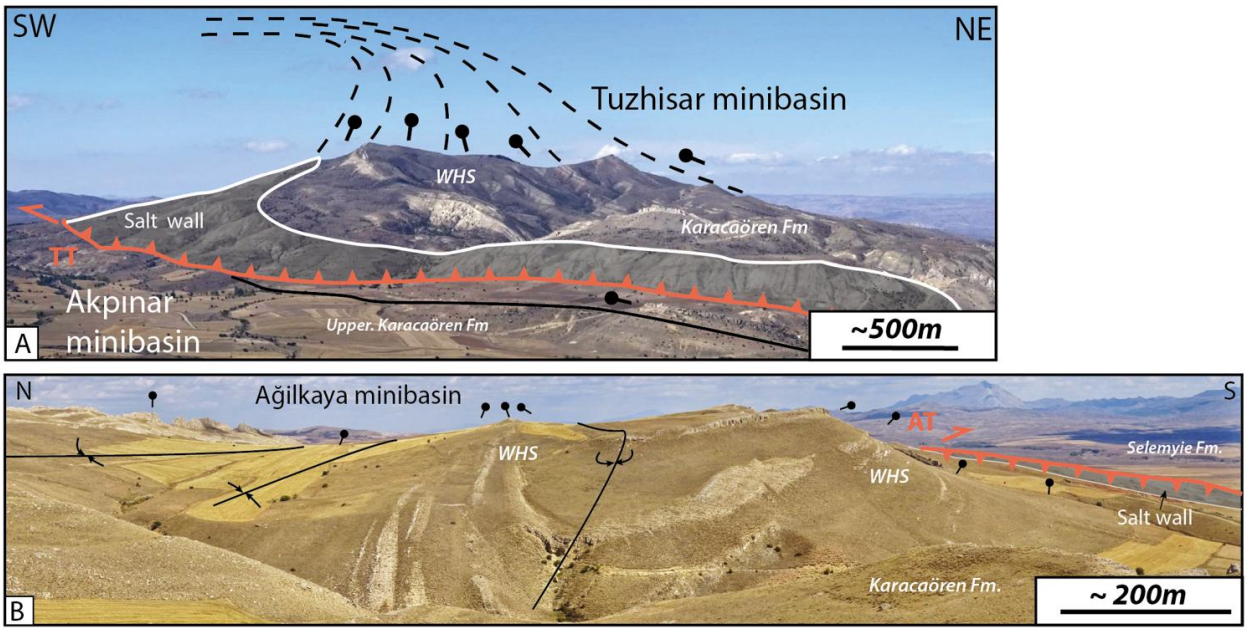
SW
NE
Tuzhisar minibasin
WHS
Salt wall
Karacaören Fm
TT
Akpınar
minibasin
Upper. Karacaören Fm
~500m
A
N
Ağilkaya minibasin
S
WHS
AT
WHS
Selemyie Fm.
Salt wall
Karacaören Fm.
~ 200m
B

Fig. 10

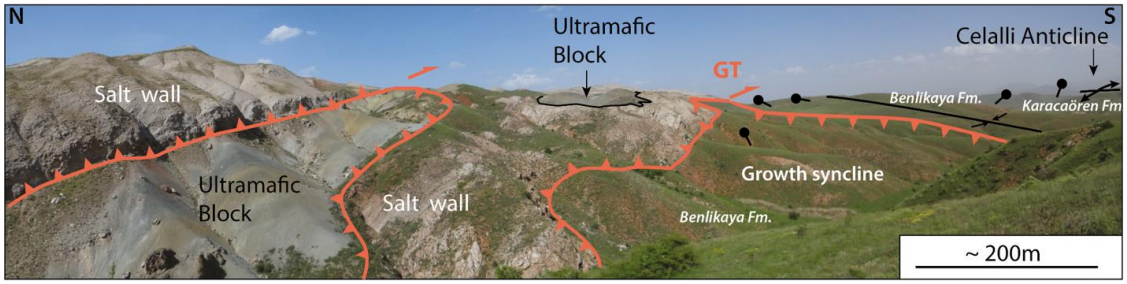
N
S
Ultramafic
Block
Celalli Anticline
GT
Salt wall
Benlikaya Fm.
Karacaören Fm
Growth syncline
Ultramafic
Block
Salt wall
Benlikaya Fm.
~ 200m

Fig. 11

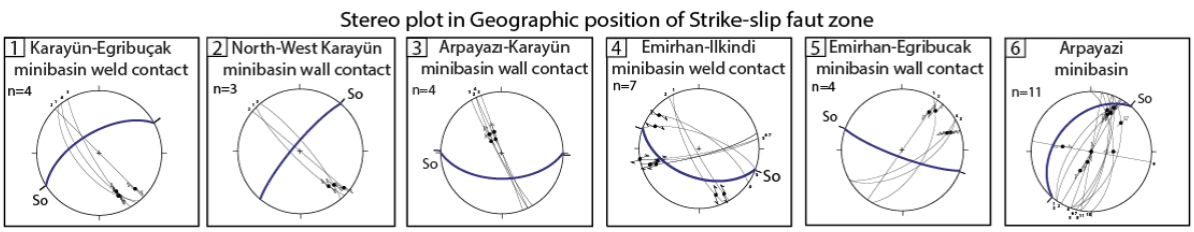
Stereo plot in Geographic position of Strike-slip faut zone
1 Karayün-Egribuçak minibasin weld contact
n=4
So
2 North-West Karayün minibasin wall contact
n=3
So
3 Arpayazı-Karayün minibasin wall contact
n=4
So
4 Emirhan-Ilkindi minibasin weld contact
n=7
So
5 Emirhan-Egribucak minibasin wall contact
n=4
So
6 Arpayazi minibasin
n=11
So

Fig. 12

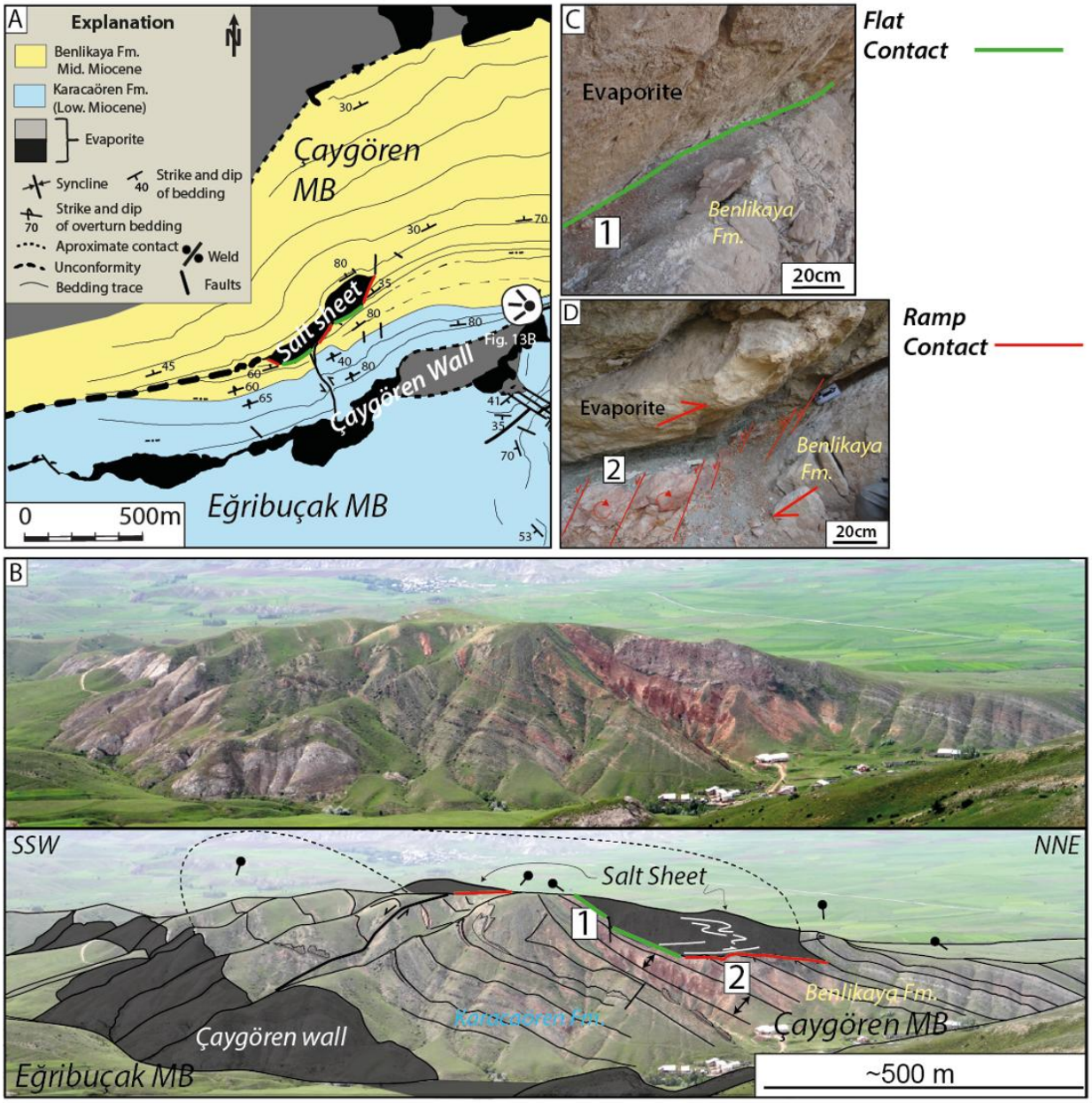
A
Explanation
Benlikaya Fm.
Mid. Miocene
Karacaören Fm.
(Low. Miocene)
Evaporite
Syncline
Strike and dip
of bedding
Strike and dip
of overturn bedding
Aproximate contact
Unconformity
Bedding trace
Weld
Faults
Çaygören
MB
Salt sheet
Çaygören Wall
Fig. 13B
Eğribuçak MB
0
500m
C
Evaporite
Benlikaya
Fm.
1
20cm
Flat
Contact
D
Evaporite
Benlikaya
Fm.
2
20cm
Ramp
Contact
B
SSW
NNE
Salt Sheet
1
2
Benlikaya Fm.
Karacaören Fm.
Çaygören MB
Çaygören wall
Eğribuçak MB
~500 m

Fig. 13

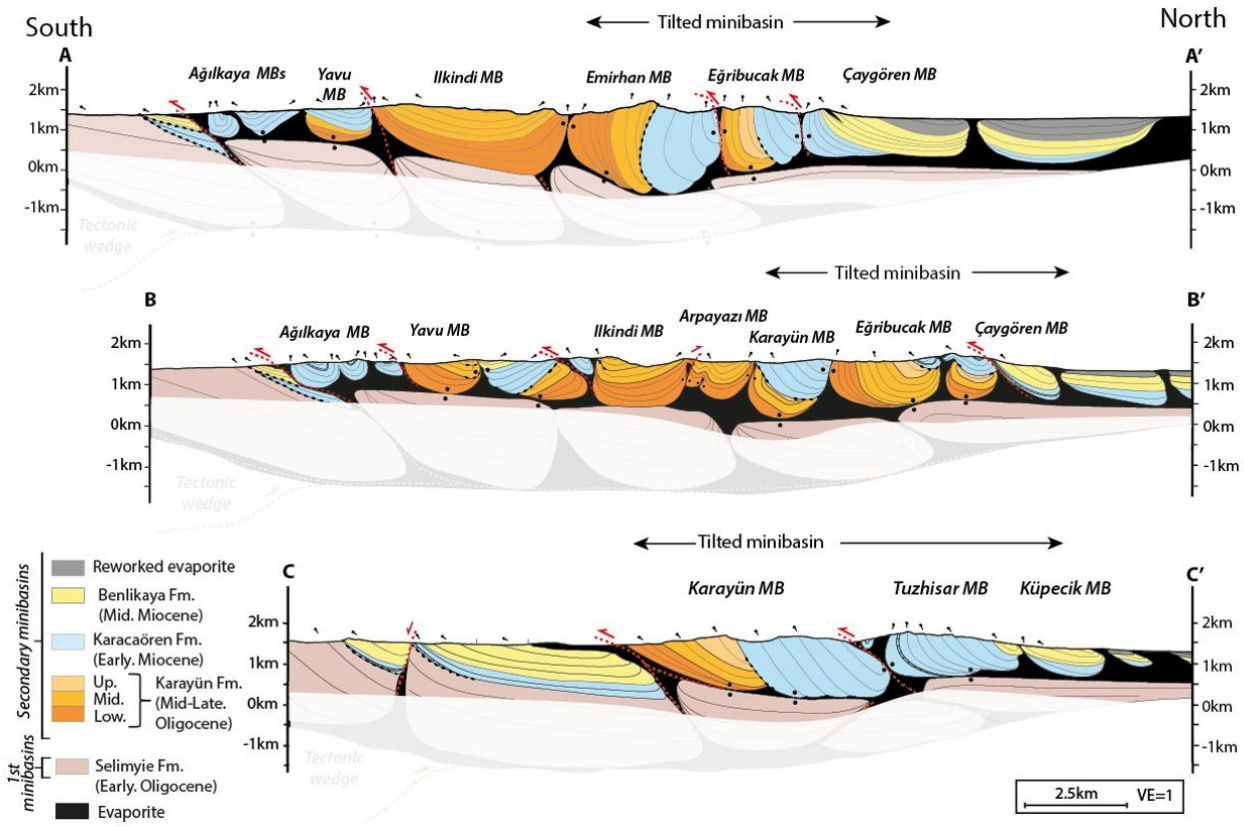
South
North
Tilted minibasin
A
A′
Ağılkaya MBs
Yavu MB
Ilkindi MB
Emirhan MB
Eğribucak MB
Çaygören MB
2km
1km
0km
-1km
Tectonic wedge
Tilted minibasin
B
B′
Ağılkaya MB
Yavu MB
Ilkindi MB
Arpayazı MB
Karayün MB
Eğribucak MB
Çaygören MB
Tilted minibasin
C
C′
Karayün MB
Tuzhisar MB
Küpecik MB
Reworked evaporite
Benlikaya Fm.
(Mid. Miocene)
Karacaören Fm.
(Early. Miocene)
Up.
Mid.
Low.
Karayün Fm.
(Mid-Late.
Oligocene)
Secondary minibasins
1st minibasins
Selimyie Fm.
(Early. Oligocene)
Evaporite
2.5km
VE=1

Fig. 14

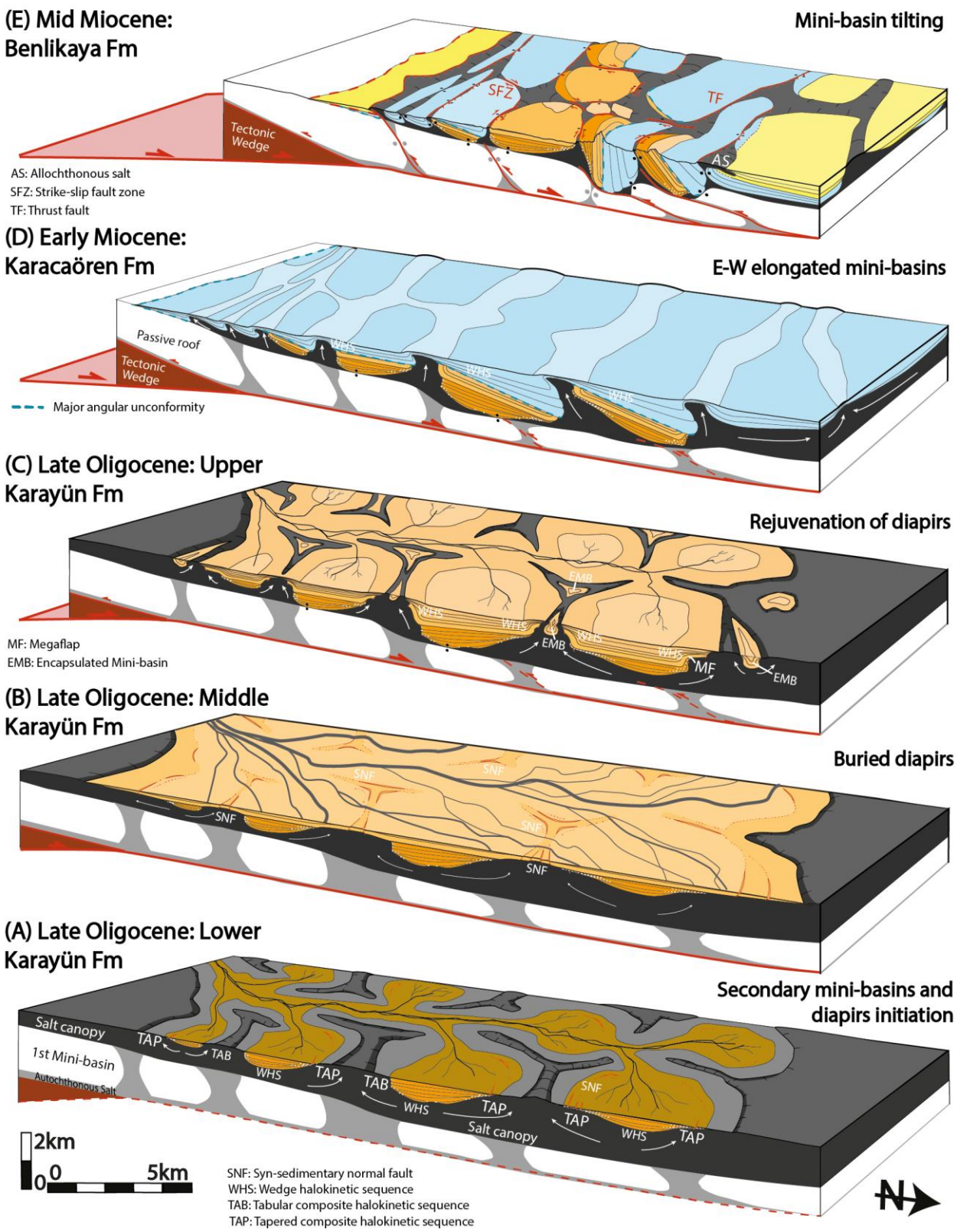
(E) Mid Miocene:
Benlikaya Fm
Mini-basin tilting
SFZ
TF
AS
Tectonic Wedge
AS: Allochthonous salt
SFZ: Strike-slip fault zone
TF: Thrust fault
(D) Early Miocene:
Karacaören Fm
E-W elongated mini-basins
Passive roof
Tectonic Wedge
WHS
Major angular unconformity
(C) Late Oligocene: Upper
Karayün Fm
Rejuvenation of diapirs
EMB
WHS
MF
MF: Megaflap
EMB: Encapsulated Mini-basin
(B) Late Oligocene: Middle
Karayün Fm
Buried diapirs
SNF
(A) Late Oligocene: Lower
Karayün Fm
Secondary mini-basins and
diapirs initiation
Salt canopy
1st Mini-basin
Autochthonous Salt
TAP
TAB
WHS
2km
0
5km
SNF: Syn-sedimentary normal fault
WHS: Wedge halokinetic sequence
TAB: Tabular composite halokinetic sequence
TAP: Tapered composite halokinetic sequence
N

Fig. 15

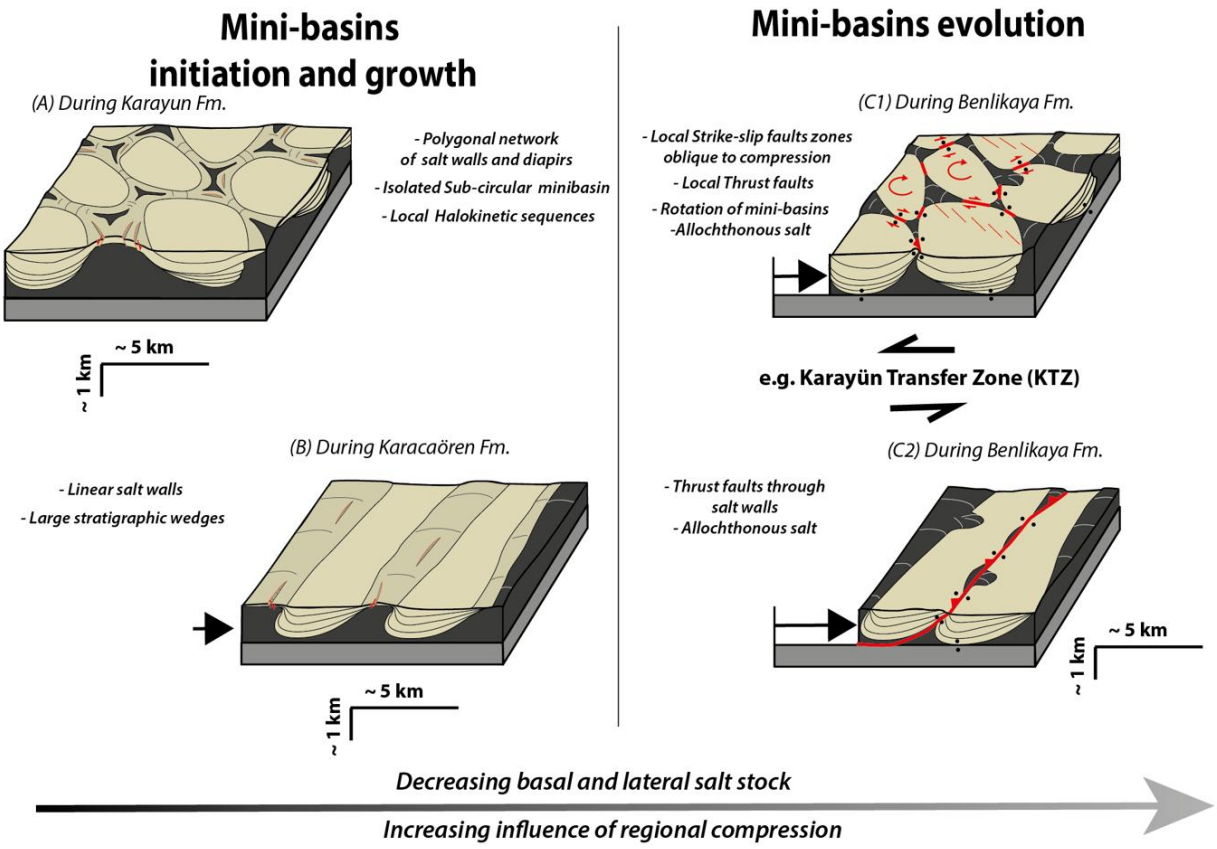
Mini-basins
initiation and growth
(A) During Karayun Fm.
- Polygonal network
of salt walls and diapirs
- Isolated Sub-circular minibasin
- Local Halokinetic sequences
~ 5 km
~ 1 km
(B) During Karacaören Fm.
- Linear salt walls
- Large stratigraphic wedges
~ 5 km
~ 1 km
Mini-basins evolution
(C1) During Benlikaya Fm.
- Local Strike-slip faults zones
oblique to compression
- Local Thrust faults
- Rotation of mini-basins
-Allochthonous salt
e.g. Karayün Transfer Zone (KTZ)
(C2) During Benlikaya Fm.
- Thrust faults through
salt walls
- Allochthonous salt
~ 5 km
~ 1 km
Decreasing basal and lateral salt stock
Increasing influence of regional compression

Fig. 16

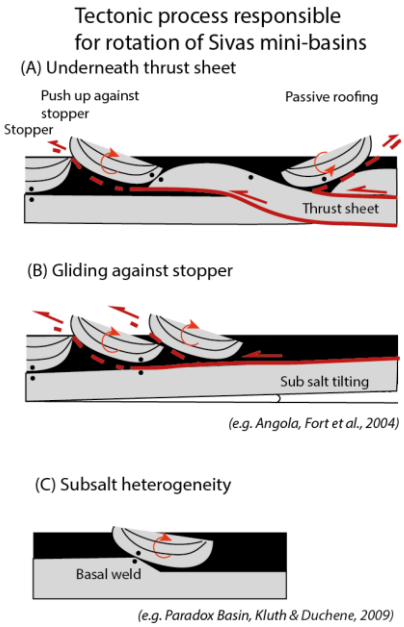
Tectonic process responsible
for rotation of Sivas mini-basins
(A) Underneath thrust sheet
Push up against
stopper
Stopper
Passive roofing
Thrust sheet
(B) Gliding against stopper
Sub salt tilting
(e.g. Angola, Fort et al., 2004)
(C) Subsalt heterogeneity
Basal weld
(e.g. Paradox Basin, Kluth & Duchene, 2009)

Fig. 17